10.1161/CIRCULATIONAHA.117.031589

Dicer in Macrophages Prevents Atherosclerosis by Promoting Mitochondrial Oxidative Metabolism

Running Title: *Wei et al.; Macrophage Dicer Prevents Atherosclerosis*

Yuanyuan Wei, PhD[1,2]; Judit Corbalán-Campos, MSc[1#]; Rashmi Gurung, MD[1#]; Lucia Natarelli, PhD[1]; Mengyu Zhu, PhD[1]; Nicole Exner, PhD[3]; Florian Erhard, PhD[4,6]; Franziska Greulich, PhD[5]; Claudia Geißler, BSc[1]; N. Henriette Uhlenhaut, PhD[5]; Ralf Zimmer, PhD[4]; Andreas Schober, MD[1,2]

[1]Experimental Vascular Medicine (EVM), Institute for Cardiovascular Prevention (IPEK), Ludwig-Maximilians-University Munich, Munich, Germany; [2]DZHK (German Center for Cardiovascular Research), Partner Site Munich Heart Alliance, Munich, Germany; [3]Biomedical Research Center, Biochemistry, Ludwig-Maximilians-University Munich, Munich, Germany; [4]Institut für Informatik, Ludwig-Maximilians-University Munich, Munich, Germany; [5]Helmholtz Diabetes Center (HMGU) and German Center for Diabetes Research (DZD), IDO, Munich, Germany; [6]Current address: Institut für Virologie, Julius-Maximilians-Universität Würzburg, Würzburg, Germany

[#]These authors contributed equally to this work.

Addresses for Correspondence:

Andreas Schober, MD
Experimental Vascular Medicine (EVM)
Institute for Cardiovascular Prevention
Ludwig-Maximilians-University Munich
Pettenkoferstr. 9b, 80336 Munich, Germany
Tel: +49-89-440055151
Fax: +49-89-440054740
Email: aschober@med.lmu.de

Yuanyuan Wei, PhD
Experimental Vascular Medicine (EVM)
Institute for Cardiovascular Prevention
Ludwig-Maximilians-University Munich
Pettenkoferstr. 9b, 80336 Munich, Germany
Tel: +49-89-440052532
Fax: +49-89-440054740
Email: Yuanyuan.Wei@med.uni-muenchen.de

Abstract

***Background*—**Alternative macrophage activation, which relies on mitochondrial oxidative metabolism, plays a central role in resolution of inflammation and prevents atherosclerosis. Moreover, macrophages handle large amounts of cholesterol and triglycerides derived from the engulfed modified lipoproteins during atherosclerosis. Although several microRNAs regulate macrophage polarization, the role of microRNA-generating enzyme Dicer in macrophage activation during atherosclerosis is unknown.

***Methods*—**To evaluate the role of Dicer in atherosclerosis, *Apoe*$^{-/-}$ mice with or without macrophage-specific *Dicer* deletion were fed a high-fat diet for 12 weeks. AGO2-RIP-ChIP, RNA deep sequencing combined with microRNA functional screening were performed in the *Dicer* wild type and knockout bone marrow-derived macrophages to identify the individual microRNAs and the mRNA targets mediating the phenotypic effects of Dicer. The role of identified individual microRNA and its target in atherosclerosis was determined by tail vein injection of the target site blockers (TSBs) in atherosclerotic *Apoe*$^{-/-}$ mice.

***Results*—**We show that *Dicer* deletion in macrophages accelerated atherosclerosis in mice along with enhanced inflammatory response and increased lipid accumulation in lesional macrophages. *In vitro*, alternative activation was limited, whereas lipid-filled 'foam cell' formation was exacerbated in *Dicer*-deficient macrophages due to impaired mitochondrial fatty acid oxidative metabolism. Rescue of miR-10a, let-7b and miR-195a expression restored the oxidative metabolism in alternatively activated *Dicer*-deficient macrophages. Suppression of ligand-dependent nuclear receptor co-repressor (Lcor) by miR-10a promoted fatty acid oxidation, which mediated the lipolytic and anti-inflammatory effect of Dicer. miR-10a expression was negatively correlated to the progression of atherosclerosis in human. Blocking the interaction between Lcor and miR-10a by TSBs aggravated atherosclerosis development in mice.

Conclusions—Dicer plays an atheroprotective role by coordinately regulating the inflammatory response and lipid metabolism in macrophages through enhancing fatty acid-fueled mitochondrial respiration, suggesting that promoting Dicer/miR-10a-dependent metabolic reprogramming in macrophages has potential therapeutic implications to prevent atherosclerosis.

Key Words: atherosclerosis; microRNA; macrophage; cellular metabolism; mitochondria; foam cell

Clinical Perspective

What is new?

- MiRNA biogenesis, *e.g.*, of the miRNAs miR-10a and let-7b, promotes the degradation of fatty acids by mitochondrial respiration in macrophages, which reduces intracellular lipid storage and limits atherosclerosis.

What are the clinical implications?

- Reducing foam cell formation in atherosclerotic arteries by enhancing energy metabolism through miRNA-mediated fatty acid oxidation may be a promising approach for the treatment of atherosclerosis.

Introduction

At bifurcations and curvatures of arteries, circulating lipoproteins, such as low-density lipoproteins (LDL), enter the vessel wall through leaky junctions frequently associated with enhanced endothelial cell turnover[1, 2]. In the subendothelial space, chemical modifications of LDL result in the unrestricted uptake of these particles by monocyte-derived macrophages through scavenger receptors, such as CD36[3]. Surplus lipids that cannot be introduced into the reverse cholesterol transport or degraded by mitochondrial β-oxidation are stored as cholesteryl ester and triglycerides in lipid droplets. Excessive lipid accumulation in lesional macrophages (a process called foam cell formation) is associated with increased oxygen consumption in early atherosclerosis, indicating a role of mitochondria in managing lipid excess by fatty acid oxidation (FAO)[4-6]. However, oxygen consumption declines during lesion progression, which may decrease the degradation of triglycerides and thereby promote macrophage apoptosis[5, 7]. The high lipid content of dead foam cells in turn poses a metabolic threat to macrophages clearing the vessel wall[8]. Engulfment of apoptotic cells upregulates ATP-binding cassette transporters ABCA1 and ABCG1 by nuclear receptors RXR heterodimers, which protects the efferocyte from apoptosis due to cholesterol overload by increasing cholesterol efflux and increases phagocytosis[9-11]. In advanced atherosclerosis, efferocytosis is defective, leading to the formation of a necrotic core consisting of cell debris and thrombogenic lipids[12]. The necrotic core characterizes vulnerable lesions that are prone to rupture and result in thrombotic obstruction of arteries[13].

Inflammatory activation of macrophages by Toll-like receptor 4 (TLR4) agonists, such as lipopolysaccharide (LPS), results in intracellular lipid storage and foam cell formation by activating the transcription factor hypoxia-inducible factor-1α, which shifts energy metabolism

from FAO and oxidative phosphorylation (OXPHOS) to glycolysis[4, 14-16]. Instead of producing ATP, mitochondria in LPS-stimulated macrophages primarily generate reactive oxygen species (ROS), which promote their pro-inflammatory state and antimicrobial activity[17, 18]. Moreover, oxygen is utilized to produce nitric oxide after LPS-induced upregulation of nitric oxide synthase 2 (NOS2)[19, 20]. By replacing oxidative energy production, glycolytic ATP synthesis protects inflammatory macrophages from cell death[21]. By contrast, alternative macrophage activation by interleukin-4 (IL-4) limits lipid droplet formation, increases oxygen consumption, FAO and OXPHOS, and promotes an anti-inflammatory phenotype[22]. IL-4 induces the transcription of genes involved in FAO and mitochondrial biogenesis through STAT6-mediated upregulation of PPAR gamma coactivator (PGC)-1β[23, 24], which is a transcriptional coactivator of PPARα and nuclear respiratory factor 1[24]. In addition, sirtuin1 (Sirt1) activates PGC-1β by deacetylation and promotes FAO in macrophages during inflammation resolution[25, 26]. The increased OXPHOS in alternatively activated macrophages (AAMs) is associated with prolonged survival, downregulation of NOS2, and improved phagocytosis[22, 27].

MicroRNAs (miRNAs) regulate macrophage activation by promoting (*e.g.*, miR-155) or inhibiting (*e.g.*, miR-223) inflammatory signaling pathways[28, 29]. Moreover, miRNAs play key roles in macrophage cholesterol metabolism, for instance through suppression of cholesterol efflux by targeting ABCA1, and are involved in foam cell formation[28]. In atherosclerosis, upregulation of miR-155 in foam cells enhances necrotic core formation by inhibiting efferocytosis[30]. The endoribonuclease Dicer produces 21-25-nucleotide long RNA duplexes by cleaving the terminal loop of precursor miRNAs and transfers the duplexes to Argonaut (Ago) proteins in the RNA-induced silencing complexes (RISCs), which are activated by removal of one of the strands of the RNA duplexes[31]. Due to the short seed sequence of 6-7 nucleotides,

miRNAs usually bind to hundreds of target mRNAs, and, conversely, one mRNA transcript can be targeted by multiple miRNAs[32]. Notably, global miRNA expression is substantially decreased in macrophages from cigarette smokers due to inhibition of Dicer by SUOMylation[33]. In mice, *Dicer* knockout increases inflammatory activation of tumor-associated macrophages[34], suggesting that Dicer may play a role in macrophage polarization. However, the concerted effect of the miRNA network in macrophages on atherosclerosis is still incompletely understood.

In the present study, we identified Dicer as a positive regulator of FAO and OXPHOS in macrophages, which promoted an AAM phenotype and limited foam cell formation. In mice, *Dicer* knockout in macrophages fostered atherosclerosis characterized by enhanced inflammation, foam cell formation, macrophage apoptosis and necrotic core formation in the lesions. Dicer generated miRNAs, like miR-10a and let-7b, which increased mitochondrial respiration by targeting co-repressors of nuclear receptors, such as ligand-dependent nuclear receptor corepressor (Lcor). Blocking the interaction between miR-10a and Lcor aggravated atherosclerosis progression in mice. Therefore, Dicer and miRNAs (such as miR-10a) integrate the immune system and lipid metabolism by promoting FAO and OXPHOS during macrophage activation through inhibiting the co-repressors of nuclear receptors, which prevents atherosclerosis.

Methods

Data disclosure statement

The data that support the findings of this study are available from the corresponding author upon reasonable request.

Animal models

To generate *Apoe*$^{-/-}$ mice containing a loxP site-flanked *Dicer* sequence[35] and a transgene with Cre recombinase under the control of the myeloid cell-specific M–lysozyme (LysM) promoter, *LysM*^{Cre} mice were crossed with *Dicer*$^{flox/flox}$/*Apoe*$^{-/-}$ mice (The Jackson Laboratory) to obtain *LysM*^{Cre}/*Dicer*$^{WT/flox}$/*Apoe*$^{-/-}$ mice. *LysM*^{Cre}/*Dicer*$^{flox/flox}$/*Apoe*$^{-/-}$ (*M-Dicer*$^{-/-}$) and *LysM*^{Cre}/*Dicer*$^{WT/WT}$/*Apoe*$^{-/-}$ (*M-Dicer*$^{+/+}$) littermates (6-8 weeks old) were fed a high-fat diet (HFD) comprising 21% crude fat (E15721-347, Ssniff) for 12 weeks. The aortas and aortic roots were harvested after *in situ* perfusion with 4% paraformaldehyde (Carl Roth), PAXgene (Qiagen) or RNAlater (Thermo Fisher Scientific) via the left ventricle. All animal experiments were reviewed and approved by the local authorities (State Agency for Nature, Environment and Consumer Protection of North Rhein-Westphalia and District Government of Upper Bavaria) in accordance with the German animal protection laws.

Transfection

Lipofectamine RNAiMAX Reagent (Thermo Fisher Scientific) was used to transfect murine bone marrow-derived macrophages (BMDMs) with mirVana miRNA mimics (30 nM; Thermo Fisher Scientific), LNA-modified miRNA inhibitors (50 nM; Exiqon), GapmeRs (50 nM; Exiqon), Target site blockers (TSBs, 50 nM; Exiqon) or scrambled controls. The sequences of miRNA inhibitors, GapmeRs and TSBs are listed in Supplemental Table 1.

AGO2-RIP-chip

The AGO2-RIP of *Dicer*$^{+/+}$ or *Dicer*$^{-/-}$ BMDMs was performed as described before[29]. Input RNA, AGO2- or IgG-immunoprecipitated (IPed) RNA were reverse transcribed and pre-amplified with Ovation PicoSL WTA System V2 (NuGEN) followed by the microarray analysis. Agilent SurePrint G3 Mouse Gene Expression microarrays (8 x 60 K format, Agilent

Technologies) were used in combination with a one-color based hybridization protocol (IMGM Laboratories GmbH). Raw signals on the microarrays were scanned using the Agilent DNA Microarray Scanner (Agilent Technologies).

To quantify the gene enrichment in AGO2-complexes, RIP-chip data were analyzed according to a method described previously[36]. Probe intensity values were estimated using Feature Extraction 10.7.3.1 software (Agilent Technologies). All arrays were quantile normalized. Enrichment values were computed for AGO2-IP against input, AGO2-IP against IgG-IP and IgG-IP against input (for our results we used the enrichment of AGO2-IP against IgG-IP). To account for differing pulldown efficiencies, a second normalization was performed on enrichment values using principal component analysis. Finally, significantly enriched genes were determined using a normal mixture modelling approach to distinguish non-associated mRNAs from mRNAs enriched in AGO2 complexes. As the background distribution of intensity values from Agilent arrays is different from Affymetrix arrays used in[36], the normal mixture models were only estimated by using probes flagged as "IsWellAboveBG". By using TargetScan 6.2 algorithms, the miRNA target sites were predicted in those mRNAs that were upregulated (cut-off: 2-fold), but less enriched at least by 50% in AGO2-complexes of *Dicer*$^{-/-}$ BMDMs compared to *Dicer*$^{+/+}$ BMDMs.

RNA-Sequencing

Total RNA was extracted from resting *Dicer*$^{+/+}$ or *Dicer*$^{-/-}$ BMDMs using the RNeasy Mini kit (Qiagen) with on-column DNase digest. 500 ng RNA was used as input to the TruSeq mRNA library preparation kit (RS-122-2103, Illumina) and sequenced on the Illumina HiSeq3000. FastQC (http://www.bioinformatics.babraham.ac.uk/projects/fastqc/) was performed for quality control. The reads were mapped to the mouse genome GRCm38.81 (mm10) and reads

overlapping genes counted simultaneously using STAR aligner version 2.4.1d[37] with the following options: *--outFilterMultimapNmax 20 --alignSJoverhangMin 8 --alignSJDBoverhangMin 1 --outFilterMismatchNmax 999 --outFilterMismatchNoverLmax 0.04 --alignIntronMin 20 --alignIntronMax 1000000 --alignMatesGapMax 100000 --quantMode GeneCounts*. DeSeq2[38] was used to identify differentially-expressed genes in *Dicer*$^{+/+}$ and *Dicer*$^{-/-}$ BMDMs. In brief, Deseq2 uses negative linearized binomial modeling to estimate the dispersion and therefore models differential expression in a data-driven way. Genes showing a mean expression of 50 counts were treated as expressed and when changed 1.5-fold (FDR < 0.05) were called differentially expressed. The pathway enrichment (absolute z-score > 2, $P < 0.05$) of the differentially expressed mRNAs was investigated by Ingenuity Pathway Analysis (Qiagen). The significance values for the pathways were calculated by one-sided Fisher's exact test.

Quantitative real-time PCR (qRT-PCR)

Total RNA was reverse-transcribed with a high-capacity cDNA reverse transcription kit or TaqMan MicroRNA Reverse Transcription Kit (Thermo Fisher Scientific). The mRNA qRT-PCR assay was performed with gene-specific primers (Supplemental Table 2) and GoTaq qPCR Master Mix (Promega). The miRNA qRT-PCR was performed with TaqMan MicroRNA Assays (Thermo Fisher Scientific). The data were normalized to a single or multiple reference genes (b2m, Gapdh and Tbp for mRNA, U6 and sno135 for miRNA), scaled to the sample with the lowest expression (qbase software, Biogazelle), and logarithmically transformed (Log10).

Human carotid lesion samples

Human atherosclerotic lesion specimens were obtained from 23 patients (mean age 75 ± 8 years; 55% were symptomatic; 35% females and 65% males) during endarterectomy. One-half of each sample was immediately stored in RNAlater for RNA isolation, and the other half was fixed in

paraformaldehyde followed by paraffin embedding and sectioning. The sections were stained with Movat's pentachrome staining and the necrotic core areas were quantified using ImageJ. The Ethics Committee of the Medical Faculty at RWTH Aachen University approved the study protocol for the collection of human atherosclerotic plaque samples, and written informed consent was obtained from all participating subjects.

***In vivo* TSB treatment**

Following 8 weeks of HFD feeding, male *Apoe*$^{-/-}$ mice (6-8 weeks old) were randomized to the different experimental groups and injected once weekly via the tail vein with miR10a/*Lcor* or control TSBs (20 mg/kg, Exiqon) for 4 weeks. During the injection period, mice were fed with a HFD. The tissues were harvested 1 week after the last injection.

Statistical analysis

Two groups were compared using unpaired Student's t-test and more than two groups were compared by one-way or two-way ANOVA depending on the number of grouping variables (Prism, GraphPad Software). For post-hoc multiple comparisons after ANOVA, the Tukey-Kramer test was used to compare every mean with every other mean and unprotected Fisher's Least Significant Difference (LSD) test was performed for planned comparisons without correction. Data from the human plaque samples were analyzed using Pearson correlation coefficient. *P* values < 0.05 were considered as statistically significant.

Data availability

The RNA sequencing, AGO2-RIP-chip and miRNA qPCR array data have been deposited in the National Center for Biotechnology Information Gene Expression Omnibus (GEO; http://www.ncbi.nlm.nih.gov/geo/) and are accessible with GEO series accession number GSE87721 (AGO2-RIP-chip and miRNA qPCR array) and GSE106854 (RNA sequencing).

Results

Dicer Deletion in Macrophages Leads to Enhanced Atherosclerosis in *Apoe*$^{-/-}$ Mice

To investigate the role of macrophage Dicer in atherosclerosis, we generated *Apoe* deficient mice with a myeloid cell-specific knockout of *Dicer* (*LysM*^{Cre}/*Dicer*$^{flox/flox}$/*Apoe*$^{-/-}$; *M-Dicer*$^{-/-}$ in brief). The null allele was confirmed in BMDMs from *M-Dicer*$^{-/-}$ mice as compared to BMDMs from *LysM*^{Cre}/*Dicer*$^{wt/wt}$/*Apoe*$^{-/-}$ (*M-Dicer*$^{+/+}$) mice (Supplemental Figure 1A). In *M-Dicer*$^{-/-}$ mice, *Dicer* mRNA expression was reduced by 94% in BMDMs and by 81% in aortic lesions after 12 weeks of HFD feeding (Supplemental Figure 1B and 1C). *M-Dicer*$^{-/-}$ mice developed more severe atherosclerosis in aortas and aortic roots, and larger necrotic core areas in the lesions than *M-Dicer*$^{+/+}$ mice (Figure 1A, 1B and Supplemental Table 3). Although lesional macrophage and smooth muscle cell contents were not changed (Supplemental Figure 1D and 1E), more lesional macrophages accumulated lipid droplets and were apoptotic in *M-Dicer*$^{-/-}$ mice than in *M-Dicer*$^{+/+}$ mice, as shown by Perilipin-2 (PLIN2) and Caspase3 immunostaining, respectively (Figure 1C, 1D and Supplemental Figure 1F). *Dicer* knockout in macrophages increased *Nos2*, *Il1b* and *Ccl2* expression and reduced *Fizz1* and *Ym1* expression in aortic arch lesions obtained by laser capture microdissection (Figure 1E). However, circulating cholesterol levels and leukocyte counts in *Apoe*$^{-/-}$ mice were not changed by *Dicer* ablation in macrophages (Supplemental Table 3). Taken together, our data indicate that macrophage Dicer prevents atherosclerosis by decreasing inflammation, lipid accumulation and apoptosis of lesional macrophages.

Dicer Promotes Alternative Macrophage Activation through Metabolic Reprogramming

Next, we studied the effect of Dicer on macrophage polarization. In resting, IL-4-, and LPS/ Interferon gamma (IFN-γ)-stimulated BMDMs, *Dicer* deficiency increased *Il1b* and *Ccl2*

expression levels, and downregulated the AAM marker *Mrc1* (Figure 2A). However, in opposite to the effect in LPS/IFN-γ-treated macrophages, *Dicer* knockout upregulated *Nos2* and *Tnf* expression and downregulated AAM markers *Fizz1* and *Ym1* expression in resting and IL-4-treated BMDMs (Figure 2A). Notably, these data indicate that *Dicer* knockout in resting macrophages and AAMs mimics the pro-inflammatory effect of *Dicer* deletion on lesional macrophages. To analyze the effect of *Dicer* knockout on signaling pathways, we performed RNA deep sequencing in resting $Dicer^{+/+}$ and $Dicer^{-/-}$ BMDMs. Pathway analysis of the 826 downregulated genes and the 910 upregulated genes (1.5-fold change cutoff, $P < 0.05$, Supplemental Table 4) by Ingenuity Pathway Analysis software showed that nuclear factor-κB (NF-κB), pattern recognition receptor (PRR), interferon and death receptor signaling pathways were activated in $Dicer^{-/-}$ BMDMs (Figure 2B). Moreover, PPARα/RXRα signaling was inhibited in $Dicer^{-/-}$ BMDMs (Figure 2B), indicating that Dicer affects mitochondrial energy metabolism in macrophages.

IL-4 stimulation increased basal respiration and the maximal respiratory capacity of BMDMs (Supplemental Figure 2A), but it did not affect the extracellular acidification rate (ECAR) compared with vehicle or LPS/IFN-γ treatment (Supplemental Figure 2B). By contrast, LPS/IFN-γ decreased the oxygen consumption rate (OCR) and enhanced the ECAR (Supplemental Figure 2A and 2B). Knockout of *Dicer* prevented the stimulatory effect of IL-4 on macrophage respiration, and slightly reduced the OCR in resting BMDMs (Figure 2C). However, *Dicer* knockout did not alter the OCR in LPS/IFN-γ-treated BMDMs (Figure 2C). In addition, deletion of *Dicer* did not affect the ECAR in resting, IL-4-, or LPS/IFN-γ-treated macrophages (Supplemental Figure 2B). Similar to the effect of *Dicer* knockout, blocking FAO by etomoxir (an inhibitor of carnitine palmitoyltransferase I) inhibited basal respiration in IL-4

stimulated BMDMs (Figure 2D). In IL-4-treated *Dicer*$^{-/-}$ BMDMs, however, etomoxir did not alter the basal OCR (Figure 2D), indicating that FAO contributes to Dicer-mediated respiration in AAMs. Moreover, increase of ATP production in IL-4-treated compared with LPS/IFN-γ-treated BMDMs was absent in *Dicer*$^{-/-}$ BMDMs (Figure 2E), and *Dicer* knockout abolished the pro-survival effect of IL-4 on macrophages (Figure 2F). In contrast to LPS/IFN-γ, IL-4 increased the expression of genes that enhance mitochondrial function (*e.g.*, *Ppargc1b*, the gene name of PGC-1β), FAO (*e.g.*, *Hadhb*), and oxidative phosphorylation (*e.g.*, *Idh3a*) (Supplemental Figure 2C). *Dicer* knockout decreased the expression of genes related to mitochondrial function, such as *Ppargc1b* and *Sirt1*, FAO, and OXPHOS (Figure 2G). In addition, mitochondrial mass (Figure 2H), mitochondrial DNA content (Supplemental Figure 2D), and the number of respiring mitochondria (Figure 2I) were reduced in IL-4-treated *Dicer*$^{-/-}$ BMDMs compared with *Dicer*$^{+/+}$ BMDMs. These data demonstrate that Dicer plays an essential role in alternative macrophage polarization by promoting mitochondrial respiration.

Dicer-Induced Oxidative Metabolism Limits Foam Cell Formation

AAMs are characterized by less lipid droplet formation and increased lipolysis of LDL-derived triglycerides compared with inflammatory macrophages[22]. Hence, we aimed to study the effect of Dicer on foam cell formation. Treatment with oxidized LDL (oxLDL) for 72 h, which results in foam cell formation, increased basal respiration and the maximal respiratory capacity in BMDMs compared with native LDL (nLDL) and vehicle treatment (Figure 3A). By contrast, oxLDL treatment for 24 h or 48 h did not affect the OCR (Supplemental Figure 3), indicating that only excessive lipid accumulation increases mitochondrial respiration. Moreover, oxLDL upregulated *Sirt1*, *Ppargc1b*, *Acox3*, *Hadha/b*, *Uqcrq*, and *Tnf* expression, and downregulated *Ym1* expression compared with nLDL (Figure 3B and 3C).

Dicer knockout limited oxLDL-induced mitochondrial respiration (Figure 3D), and upregulation of *Sirt1*, *Ppargc1b*, *Acox3*, *Hadhb*, and *Uqcrq* expression (Figure 3E), whereas increased lipid accumulation (Figure 3F) in BMDM-derived foam cells. *Fizz1* expression was reduced in *Dicer*$^{-/-}$ BMDMs compared with the wild type control after oxLDL treatment (Figure 3C). Moreover, blocking the transport of fatty acyl chains into mitochondria using etomoxir decreased the OCR (Figure 3G) and enhanced the lipid accumulation in oxLDL-treated BMDMs (Figure 3F). The effect of etomoxir on foam cell formation was absent in *Dicer*$^{-/-}$ BMDMs (Figure 3F). These findings indicate that excessive lipid accumulation in macrophages is balanced by Dicer-induced oxidative metabolism of fatty acids.

Dicer Drives Macrophage Metabolic Reprogramming by Suppressing Lcor and Ncor2

To determine miRNA targets regulated by *Dicer* knockout, we performed miRNA qPCR array and AGO2-RIP-chip analysis in *Dicer*$^{-/-}$ BMDMs and *Dicer*$^{+/+}$ BMDMs. *Dicer* deletion resulted in downregulation of 137 miRNAs, including miRNAs highly expressed in macrophages, such as miR-146a, miR-223, let-7 miRNA family members, and miR-142-3p[28] (Figure 4A and Supplemental Table 5). Enrichment of AGO2 protein in the AGO2-immunoprecipitate, but not in the IgG-immunoprecipitate was confirmed (Supplemental Figure 4A). We found that 96 mRNAs were both enriched in the RISC of *Dicer*$^{+/+}$ BMDMs compared with that of *Dicer*$^{-/-}$ BMDMs and upregulated by *Dicer* knockout in BMDMs (Supplemental Table 6). Among those 96 genes, 67 mRNAs contained conserved binding sites for the miRNAs downregulated in *Dicer*$^{-/-}$ BMDMs as predicted by the TargetScan algorithm (Figure 4B). The highest number of conserved miRNA binding sites (*e.g.*, for miR-10a/b, let-7, miR-30, and miR-195) was predicted in the 3′-UTR of ligand-dependent nuclear receptor co-repressor (Lcor) mRNA (Figure 4B), which encodes for a protein that interacts with RXRα[39]. Binding sites for miR-10 and miR-30

family members were also predicted in the nuclear receptor co-repressor 2 (*Ncor2*) mRNA (Figure 4B), which translates into a protein that inhibits PPARα activation and mitochondrial oxidative metabolism[40]. Enrichment of *Lcor* and *Ncor2* in the RISC of *Dicer*$^{+/+}$ compared with *Dicer*$^{-/-}$ BMDMs was confirmed by qRT-PCR (Figure 4C). IL-4 downregulated *Ncor2* and oxLDL downregulated *Lcor* and *Ncor2*, which was prevented by *Dicer* knockout in BMDMs (Figure 4D, 4E and Supplemental Figure 4B). *In vivo*, *Lcor* and *Ncor2* mRNA levels were higher in atherosclerotic lesions of *M-Dicer*$^{-/-}$ mice than in those from *M-Dicer*$^{+/+}$ mice (Figure 4F). LCoR and NCoR2 were mainly detected in the nucleus of lesional macrophages by immunostaining and the nuclear localization of LCoR and NcoR2 was more prominent in *M-Dicer*$^{-/-}$ mice than in *M-Dicer*$^{+/+}$ mice (Supplemental Figure 4C and 4D).

To study the role of Lcor and Ncor2 in Dicer-mediated mitochondrial energy metabolism, *Lcor* or *Ncor2* was silenced in IL-4-treated *Dicer*$^{-/-}$ BMDMs by locked nucleic acid (LNA)-modified GapmeRs. *Lcor* knockdown (Supplemental Figure 5) increased basal respiration and maximal respiratory capacity (Figure 4G), upregulated *Sirt1*, *Ppargc1b* and *Fizz1* expression (Figure 4H), and reduced the number of non-respiring mitochondria (Figure 4I). *Ncor2* knockdown (Supplemental Figure 5) upregulated *Ppargc1b* and *Fizz1* expression (Figure 4H), whereas reduced the number of non-respiring mitochondria (Figure 4I). Next we studied the effect of LCoR on the transcriptional activity of RXRα. We transfected HEK293T cells with a vector containing the luciferase gene controlled by RXR transcriptional response elements and a vector expressing RXRα. Overexpression of Lcor inhibited luciferase activity in 9-cis-retinoic acid-treated cells, indicating that Lcor inhibits RXRα activity (Figure 4J). Treatment of IL-4-treated *Dicer*$^{-/-}$ BMDMs with the RXRα agonist CD3254 increased *Fizz1* and *Ym1* expression

(Figure 4K). These data indicate that Dicer promotes mitochondrial oxidative metabolism in macrophages by suppressing Lcor and Ncor2.

miR-10a and let-7b Mediate the Effect of Dicer on Macrophage Oxidative Metabolism

To determine miRNAs that are responsible for the phenotype of *Dicer*$^{-/-}$ macrophages, we studied the role of 13 miRNAs downregulated in *Dicer*$^{-/-}$ macrophages and predicted to target Lcor in the cellular oxygen consumption of AAMs. Transfection of miR-10a, let-7b or miR-195a mimics increased mitochondrial respiration in IL-4-treated *Dicer*$^{-/-}$ BMDMs (Figure 5A). By contrast, miR-103, let-7a/i, miR-98 or miR-200b mimic treatment did not affect and miR-30a, miR-106b, miR-142, miR-101 or miR-301 decreased the OCR in *Dicer*$^{-/-}$ BMDMs (Supplemental Figure 6). These findings suggest that Dicer promotes metabolic reprogramming of AAMs by generating miR-10a, let-7b and miR-195a.

To determine the binding sites of these 3 miRNAs in the 3′-UTR of *Lcor*, we transfected HEK293T cells with a luciferase reporter vector containing the 3′-UTR of murine *Lcor*. Transfection of miR-10a and let-7b, but not of miR-195a mimics reduced luciferase activities (Figure 5B, 5C and Supplemental Figure 7A). Mutating the miR-10a and let-7b target site in *Lcor* 3′-UTR prevented the suppression of luciferase activities by miR-10a and let-7b mimics, respectively (Figure 5B, 5C and Supplemental Figure 7B). In addition, we studied whether miR-10a targets the 3′-UTR of *Ncor2* (Supplemental Figure 7B). Transfection of miR-10a mimics reduced luciferase activities in cells expressing the luciferase reporter gene fused to the wild-type 3′-UTR of *Ncor2* (Figure 5B). This effect was absent when the miR-10a target site in *Ncor2* 3′-UTR was mutated (Figure 5B and Supplemental Figure 7B). Gain-and-loss-of-function experiments showed that let-7b and miR-195a inhibit *Lcor* expression, and miR-10a suppresses *Lcor* and *Ncor2* expression in IL-4-treated BMDMs (Figure 5D and 5E).

We then studied the role of *Dicer* in the regulation of miR-10a and let-7b expression levels in lesional macrophages. In contrast to *M-Dicer*$^{+/+}$ mice, miR-10a and let-7b expression was reduced in lesional macrophages, as determined by combined *in situ* PCR and MAC2 immunostaining (Figure 5F), and in atherosclerotic aortas (Figure 5G) from *M-Dicer*$^{-/-}$ mice. In humans, miR-10a and let-7b expression levels were lower in carotid plaques than that in the vessel wall (Figure 5H), and negatively correlated with the necrotic core area in carotid lesions (Figure 5I). These data suggest an atheroprotective role of miR-10a and let-7b expression in macrophages.

miR-10a Promotes Oxidative Metabolism by Targeting Lcor and Ncor2

Next, we studied the mechanisms by which miR-10a and let-7b affect metabolism during macrophage polarization. IL-4 and LPS/IFN-γ treatment upregulated and downregulated let-7b expression in BMDMs, respectively, but did not change miR-10a expression (Supplemental Figure 7C). miR-10a inhibition reduced *Ppargc1b*, *Fizz1* and *Ym1* expression (Figure 6A), and inhibition of let-7b downregulated *Sirt1*, *Ppargc1b*, *Mrc1* and *Ym1* expression (Figure 6B) in IL-4-treated *Dicer*$^{+/+}$ BMDMs.

LNA-modified oligonucleotides (target site blockers; TSBs) were designed to block the interaction between miR-10a and *Lcor* (miR10a/*Lcor* TSBs) or *Ncor2* (miR10a/*Ncor2* TSBs), and between let-7b and *Lcor* (let7b/*Lcor* TSBs). We found that the TSBs specifically upregulated the expression of either *Lcor* or *Ncor2* in BMDMs (Supplemental Figure 7D). Transfection of miR10a/*Lcor* TSBs reduced the expression of *Sirt1*, *Ppargc1b*, *Fizz1* and *Ym1*, whereas transfection of miR10a/*Ncor2* TSBs reduced the expression of *Ppargc1b*, *Mrc1* and *Fizz1* in IL-4-treated BMDMs (Figure 6C and 6D). Treatment with let7b/*Lcor* TSBs downregulated *Fizz1* and increased *Mrc1* and *Ym1* expression, but did not alter *Sirt1* and *Ppargc1b* expression (Figure

6E). Treatment with CD3254 prevented miR10a/*Lcor* TSB-induced downregulation of *Sirt1* and *Ppargc1b*, and miR10a/*Ncor2* TSB-induced downregulation of *Ppargc1b*, *Mrc1* and *Fizz1* expression in IL-4-treated BMDMs (Figure 6F). Moreover, miR10a/*Lcor* TSBs or let7b/*Lcor* TSBs upregulated *Mrc1*, *Fizz1* and *YM1* expression in BMDMs treated with CD3254 (Figure 6F).

In addition, transfection with miR10a/*Lcor* TSBs and to a lesser extent with miR10a/*Ncor2* TSBs, but not with let7b/*Lcor* TSBs reduced the basal OCR (Figure 6G) and cell survival (Figure 6H) of IL-4-treated BMDMs. In oxLDL-treated BMDMs, transfection with miR10a/*Lcor* TSBs or miR10a/*Ncor2* TSBs decreased the basal OCR (Figure 6I), reduced *Sirt1* and *Ppargc1b* expression (Figure 6J), and enhanced lipid accumulation (Figure 6K). Taken together, these results suggest that miR-10a contributes to the effect of Dicer on mitochondrial respiration in AAMs and foam cells by targeting Lcor and Ncor2.

Therefore, we investigated the role of miR-10a-mediated suppression of Lcor in atherosclerosis. Treatment of *Apoe*$^{-/-}$ mice with miR10a/*Lcor* TSBs during the last 4 weeks of a 12-week HFD feeding program increased atherosclerotic lesion formation in the aortic arch compared with control TSBs (Figure 6L). Moreover, miR10a/*Lcor* TSB treatment reduced *Sirt1*, *Ppargc1b*, *Mrc1*, and *Ym1* expression and increased *Lcor*, *Nos2*, *Tnf* and *Ccl2* expression in the aorta (Figure 6M). Injection of miR10a/*Lcor* TSBs increased the nuclear accumulation of LCoR in lesional macrophages (Supplemental Figure 7E). The body weights, circulating leukocyte counts and blood cholesterol levels did not differ between the groups (Supplemental Table 7). Hence, miR-10a may limit atherosclerotic lesion formation by suppressing *Lcor* in macrophages.

Discussion

Our results show that miRNA biogenesis by Dicer plays a key role in the metabolic adaptation of macrophages to excessive fatty acid availability. Dicer increased mitochondrial fatty acid oxidative capacity in AAMs and foam cells by generating miRNAs, such as miR-10a, that promoted the expression of genes involved in mitochondrial oxidative metabolism by targeting Lcor. Dicer-mediated fatty acid degradation in macrophages reduced foam cell formation and lipotoxic stress, and limited the progression of atherosclerosis to vulnerable lesions (Supplemental Figure 8).

In contrast to store fatty acids as triglycerides in lipid droplets in inflammatory macrophages, increased fatty acid availability through lysosomal lipolysis in AAMs results in enhanced OXPHOS and FAO[22], which increases ATP production, and enhances cell survival and phagocytosis[22, 27]. Moreover, mitochondrial ATP production in AAMs is associated with decreased mitochondrial ROS production and thus promotes an anti-inflammatory state[18, 41]. We found that Dicer plays an essential role in the metabolic programming of IL-4-induced AAM polarization by enhancing mitochondrial biogenesis, OXPHOS, and ATP production. As a result, Dicer reduced inflammatory signaling and cytokine production in AAMs, similar as in tumor-associated macrophages[34]. *In vivo*, myeloid cell-specific *Dicer* knockout induced a phenotypic shift of lesional macrophages towards a pro-inflammatory state, indicating that Dicer-mediated metabolic programming of AAMs limits the progression of atherosclerosis. Notably, increased oxygen consumption of macrophage-derived foam cells in early lesions ceases in advanced atherosclerosis[5]. Our findings reveal that excess lipid storage in foam cells triggers Dicer-mediated fatty acid degradation by mitochondrial respiration to reduce the triglyceride content in lipid droplets[4]. Thus, FAO and OXPHOS may protect lesional foam cells during early

atherosclerosis from lipotoxicity due to the accumulation of triglycerides[7], whereas the shutdown of mitochondrial respiration in lesional macrophages during inflammatory polarization may result in foam cell death and necrotic core formation. Conversely, decreased fatty acid synthesis in macrophages limits triglyceride and cholesteryl ester accumulation, and reduces foam cell formation in atherosclerosis[42]. Taken together, our findings indicate that Dicer expression in macrophages limits advanced atherosclerosis by increasing mitochondrial fatty acid degradation in foam cells. In contrast to its role in macrophages, endothelial Dicer promotes atherosclerosis by enhancing early monocyte recruitment[43]. Thus, the net effect of Dicer in the different cell types may strongly depend on the stage of atherosclerosis.

To investigate the mechanism by which Dicer promotes oxidative metabolism, we analyzed the miRNA targets in macrophages. We found that two nuclear receptor co-repressors, Lcor and Ncor2, mediate the effect of *Dicer* knockout on mitochondrial respiration in AAMs. Notably, interaction with Ncor2 inhibits the activity of PPARs, such as PPARα that positively regulates the expression of *Ppargc1b*, *Sirt1* and genes involved in FAO and OXPHOS[44-46], and thereby reduces mitochondrial oxidative metabolism and increases the triglyceride content in adipocytes[40]. Hence, our results indicate a similar role of Ncor2 in mitochondrial function in AAMs. Moreover, Lcor attenuates agonist-activated nuclear receptor signaling, *e.g.*, the estrogen receptor alpha and vitamin D receptor, by HDAC-dependent and -independent mechanisms[39]. In addition, Lcor promotes Kruppel-like factor 6-mediated transcriptional repression of target genes[47]. We found that Lcor interacts with RXRα and inhibits RXR activity. RXRα acts as a sensor for mitochondrial function and upregulates mitochondrial genes by interacting with PGC-1[48].

Among the miRNAs downregulated by *Dicer* knockout, miR-10a, let-7b and miR-195a enhanced cellular oxygen consumption and suppressed Lcor expression, indicating that these three miRNAs contribute to the effect of Dicer in macrophages. In addition to target Ncor2, which is in line with previous reports[49], miR-10a directly targets Lcor and thereby promotes mitochondrial function and an anti-inflammatory macrophage phenotype. Inhibition of this mechanism may play a key role in the pro-atherogenic and pro-inflammatory effect of TSBs that block the interaction between miR-10a and Lcor. Accordingly, miR-10a inhibits inflammatory monocyte activation by downregulating several components of NF-κB pathway[50]. In contrast to miR-10a, the effect of let-7b on oxidative metabolism in macrophages was not meditated through targeting Lcor, indicating that other let-7b targets are involved in the regulation of macrophage metabolic reprogramming. Other let-7 family members, like let-7a, let-7i and miR-98, did not affect metabolic reprogramming in AAMs, suggesting that the seed sequence is not essential for the let-7 effect in macrophages. Accordingly, the finding that let-7d partially mediates the effect of Dicer on polarization of tumor-associated macrophages may be due to a different mechanism[34]. miR-195, the third miRNA that mediated the effect of Dicer on macrophage metabolism, suppressed Lcor not through direct targeting of its 3′-UTR. Hence, yet unknown miR-195 targets may promote Lcor expression and inhibit mitochondrial function.

In conclusion, our findings demonstrate a critical role of Dicer in enhancing mitochondrial oxidative metabolism during alternative macrophage activation and foam cell formation by suppressing nuclear receptor co-repressor Lcor through miR-10a, indicating that miRNAs coordinate the inflammatory response and lipid metabolism in macrophages by regulating mitochondrial function.

Acknowledgments

We thank J. Grommes (European Vascular Center Aachen-Maastricht, RWTH Aachen University) for providing the human carotid plaque samples. We thank K. Heyll and L. Ruiz-Heinrich for technical assistance.

Sources of Funding

A.S. acknowledges support from the Deutsche Forschungsgemeinschaft (SFB 1123-B4), the DZHK (German Centre for Cardiovascular Research) (MHA VD 1.2), and the German Federal Ministry of Education and Research (01KU1213A). A.S. and Y.W. acknowledge support from Else Kröner-Fresenius-Stiftung (2014_A219). Y.W. acknowledges support from the DZHK (German Centre for Cardiovascular Research) (FKZ 81X2600240) and the Deutsche Forschungsgemeinschaft (WE 6160/1-1). F.G. and N.H.U acknowledge support from the Deutsche Forschungsgemeinschaft (UH275/1-1) and F.G. acknowledges support from a Daimler Benz Scholarship. F.E. and R.Z. acknowledge support from the Deutsche Forschungsgemeinschaft (SFB 1123-Z2).

Disclosures

The authors declare no conflict of interest.

References

1. Schober A, Weber C. Mechanisms of microrna s in atherosclerosis. *Annu. Rev. Pathol.* 2016;11:583-616. doi: 10.1146/annurev-pathol-012615-044135.
2. Tarbell JM. Mass transport in arteries and the localization of atherosclerosis. *Annu. Rev. Biomed. Eng.* 2003;5:79-118. doi: 10.1146/annurev.bioeng.5.040202.121529.
3. Canton J, Neculai D, Grinstein S. Scavenger receptors in homeostasis and immunity. *Nat. Rev. Immunol*. 2013;13:621-634. doi: 10.1038/nri3515.
4. Malandrino MI, Fucho R, Weber M, Calderon-Dominguez M, Mir JF, Valcarcel L, Escote X, Gomez-Serrano M, Peral B, Salvado L, Fernandez-Veledo S, Casals N, Vazquez-Carrera M, Villarroya F, Vendrell JJ, Serra D, Herrero L. Enhanced fatty acid oxidation in adipocytes and macrophages reduces lipid-induced triglyceride accumulation and inflammation. *Am. J. Physiol. Endocrinol. Metab.* 2015;308:E756-E769. doi: 10.1152/ajpendo.00362.2014.
5. Bjornheden T, Bondjers G. Oxygen consumption in aortic tissue from rabbits with diet-induced atherosclerosis. *Arteriosclerosis*. 1987;7:238-247.
6. Aon MA, Bhatt N, Cortassa SC. Mitochondrial and cellular mechanisms for managing lipid excess. *Front Physiol*. 2014;5:282. doi: 10.3389/fphys.2014.00282.
7. Aflaki E, Radovic B, Chandak PG, Kolb D, Eisenberg T, Ring J, Fertschai I, Uellen A, Wolinski H, Kohlwein SD, Zechner R, Levak-Frank S, Sattler W, Graier WF, Malli R, Madeo F, Kratky D. Triacylglycerol accumulation activates the mitochondrial apoptosis pathway in macrophages. *J. Biol. Chem.* 2011;286:7418-7428. doi: 10.1074/jbc.M110.175703.
8. Henson PM. Cell removal: Efferocytosis. *Annu. Rev. Cell Dev. Biol.* 2017;33:127-144. doi: 10.1146/annurev-cellbio-111315-125315.
9. Hamon Y, Broccardo C, Chambenoit O, Luciani MF, Toti F, Chaslin S, Freyssinet JM, Devaux PF, McNeish J, Marguet D, Chimini G. Abc1 promotes engulfment of apoptotic cells and transbilayer redistribution of phosphatidylserine. *Nat. Cell Biol.* 2000;2:399-406. doi: 10.1038/35017029.
10. Roszer T. Transcriptional control of apoptotic cell clearance by macrophage nuclear receptors. *Apoptosis*. 2017;22:284-294. doi: 10.1007/s10495-016-1310-x.
11. Yvan-Charvet L, Pagler TA, Seimon TA, Thorp E, Welch CL, Witztum JL, Tabas I, Tall AR. Abca1 and abcg1 protect against oxidative stress-induced macrophage apoptosis during efferocytosis. *Circ. Res.* 2010;106:1861-1869. doi: 10.1161/circresaha.110.217281.
12. Tabas I, Bornfeldt KE. Macrophage phenotype and function in different stages of atherosclerosis. *Circ. Res.* 2016;118:653-667. doi: 10.1161/CIRCRESAHA.115.306256.
13. Narula J, Nakano M, Virmani R, Kolodgie FD, Petersen R, Newcomb R, Malik S, Fuster V, Finn AV. Histopathologic characteristics of atherosclerotic coronary disease and implications of the findings for the invasive and noninvasive detection of vulnerable plaques. *J. Am. Coll. Cardiol.* 2013;61:1041-1051. doi: 10.1016/j.jacc.2012.10.054.
14. Feingold KR, Shigenaga JK, Kazemi MR, McDonald CM, Patzek SM, Cross AS, Moser A, Grunfeld C. Mechanisms of triglyceride accumulation in activated macrophages. *J. Leukoc. Biol.* 2012;92:829-839. doi: 10.1189/jlb.1111537.

15. Huang YL, Morales-Rosado J, Ray J, Myers TG, Kho T, Lu M, Munford RS. Toll-like receptor agonists promote prolonged triglyceride storage in macrophages. *J. Biol. Chem.* 2014;289:3001-3012. doi: 10.1074/jbc.M113.524587.
16. Pearce EL, Pearce EJ. Metabolic pathways in immune cell activation and quiescence. *Immunity*. 2013;38:633-643. doi: 10.1016/j.immuni.2013.04.005.
17. West AP, Brodsky IE, Rahner C, Woo DK, Erdjument-Bromage H, Tempst P, Walsh MC, Choi Y, Shadel GS, Ghosh S. Tlr signalling augments macrophage bactericidal activity through mitochondrial ros. *Nature*. 2011;472:476-480. doi: 10.1038/nature09973.
18. Mills EL, Kelly B, Logan A, Costa AS, Varma M, Bryant CE, Tourlomousis P, Dabritz JH, Gottlieb E, Latorre I, Corr SC, McManus G, Ryan D, Jacobs HT, Szibor M, Xavier RJ, Braun T, Frezza C, Murphy MP, O'Neill LA. Succinate dehydrogenase supports metabolic repurposing of mitochondria to drive inflammatory macrophages. *Cell*. 2016;167:457-470. doi: 10.1016/j.cell.2016.08.064.
19. Takeda N, O'Dea EL, Doedens A, Kim JW, Weidemann A, Stockmann C, Asagiri M, Simon MC, Hoffmann A, Johnson RS. Differential activation and antagonistic function of hif-{alpha} isoforms in macrophages are essential for no homeostasis. *Genes Dev.* 2010;24:491-501. doi: 10.1101/gad.1881410.
20. Kelly B, O'Neill LA. Metabolic reprogramming in macrophages and dendritic cells in innate immunity. *Cell Res.* 2015;25:771-784. doi: 10.1038/cr.2015.68.
21. Everts B, Amiel E, van der Windt GJ, Freitas TC, Chott R, Yarasheski KE, Pearce EL, Pearce EJ. Commitment to glycolysis sustains survival of no-producing inflammatory dendritic cells. *Blood*. 2012;120:1422-1431. doi: 10.1182/blood-2012-03-419747.
22. Huang SC, Everts B, Ivanova Y, O'Sullivan D, Nascimento M, Smith AM, Beatty W, Love-Gregory L, Lam WY, O'Neill CM, Yan C, Du H, Abumrad NA, Urban JF, Jr., Artyomov MN, Pearce EL, Pearce EJ. Cell-intrinsic lysosomal lipolysis is essential for alternative activation of macrophages. *Nat. Immunol*. 2014;15:846-855. doi: 10.1038/ni.2956.
23. Vats D, Mukundan L, Odegaard JI, Zhang L, Smith KL, Morel CR, Wagner RA, Greaves DR, Murray PJ, Chawla A. Oxidative metabolism and pgc-1beta attenuate macrophage-mediated inflammation. *Cell Metab*. 2006;4:13-24. doi: 10.1016/j.cmet.2006.05.011.
24. St-Pierre J, Lin J, Krauss S, Tarr PT, Yang R, Newgard CB, Spiegelman BM. Bioenergetic analysis of peroxisome proliferator-activated receptor gamma coactivators 1alpha and 1beta (pgc-1alpha and pgc-1beta) in muscle cells. *J. Biol. Chem.* 2003;278:26597-26603. doi: 10.1074/jbc.M301850200.
25. Liu TF, Vachharajani VT, Yoza BK, McCall CE. Nad+-dependent sirtuin 1 and 6 proteins coordinate a switch from glucose to fatty acid oxidation during the acute inflammatory response. *J. Biol. Chem.* 2012;287:25758-25769. doi: 10.1074/jbc.M112.362343.
26. Kelly TJ, Lerin C, Haas W, Gygi SP, Puigserver P. Gcn5-mediated transcriptional control of the metabolic coactivator pgc-1beta through lysine acetylation. *J. Biol. Chem.* 2009;284:19945-19952. doi: 10.1074/jbc.M109.015164.
27. Chandak PG, Radovic B, Aflaki E, Kolb D, Buchebner M, Frohlich E, Magnes C, Sinner F, Haemmerle G, Zechner R, Tabas I, Levak-Frank S, Kratky D. Efficient phagocytosis requires triacylglycerol hydrolysis by adipose triglyceride lipase. *J. Biol. Chem.* 2010;285:20192-20201. doi: 10.1074/jbc.M110.107854.

28. Wei Y, Schober A. Microrna regulation of macrophages in human pathologies. *Cell Mol. Life Sci.* 2016;73:3473-3495. doi: 10.1007/s00018-016-2254-6.
29. Wei Y, Nazari-Jahantigh M, Chan L, Zhu M, Heyll K, Corbalan-Campos J, Hartmann P, Thiemann A, Weber C, Schober A. The microrna-342-5p fosters inflammatory macrophage activation through an akt1- and microrna-155-dependent pathway during atherosclerosis. *Circulation*. 2013;127:1609-1619. doi: 10.1161/CIRCULATIONAHA.112.000736.
30. Wei Y, Zhu M, Corbalan-Campos J, Heyll K, Weber C, Schober A. Regulation of csf1r and bcl6 in macrophages mediates the stage-specific effects of microrna-155 on atherosclerosis. *Arterioscler. Thromb. Vasc. Biol*. 2015;35:796-803. doi: 10.1161/ATVBAHA.114.304723.
31. Ha M, Kim VN. Regulation of microrna biogenesis. *Nat. Rev. Mol. Cell Biol*. 2014;15:509-524. doi: 10.1038/nrm3838.
32. Helwak A, Kudla G, Dudnakova T, Tollervey D. Mapping the human mirna interactome by clash reveals frequent noncanonical binding. *Cell*. 2013;153:654-665. doi: 10.1016/j.cell.2013.03.043.
33. Gross TJ, Powers LS, Boudreau RL, Brink B, Reisetter A, Goel K, Gerke AK, Hassan IH, Monick MM. A microrna processing defect in smokers' macrophages is linked to sumoylation of the endonuclease dicer. *J. Biol. Chem.* 2014;289:12823-12834. doi: 10.1074/jbc.M114.565473.
34. Baer C, Squadrito ML, Laoui D, Thompson D, Hansen SK, Kiialainen A, Hoves S, Ries CH, Ooi CH, De Palma M. Suppression of microrna activity amplifies ifn-gamma-induced macrophage activation and promotes anti-tumour immunity. *Nat. Cell Biol*. 2016;18:790-802. doi: 10.1038/ncb3371.
35. Harfe BD, McManus MT, Mansfield JH, Hornstein E, Tabin CJ. The rnaseiii enzyme dicer is required for morphogenesis but not patterning of the vertebrate limb. *Proc. Natl. Acad. Sci. U. S. A.* 2005;102:10898-10903. doi: 10.1073/pnas.0504834102.
36. Erhard F, Dolken L, Zimmer R. Rip-chip enrichment analysis. *Bioinformatics*. 2013;29:77-83. doi: 10.1093/bioinformatics/bts631.
37. Dobin A, Davis CA, Schlesinger F, Drenkow J, Zaleski C, Jha S, Batut P, Chaisson M, Gingeras TR. Star: Ultrafast universal rna-seq aligner. *Bioinformatics*. 2013;29:15-21. doi: 10.1093/bioinformatics/bts635.
38. Love MI, Huber W, Anders S. Moderated estimation of fold change and dispersion for rna-seq data with deseq2. *Genome Biol.* 2014;15:550. doi: 10.1186/s13059-014-0550-8.
39. Fernandes I, Bastien Y, Wai T, Nygard K, Lin R, Cormier O, Lee HS, Eng F, Bertos NR, Pelletier N, Mader S, Han VK, Yang XJ, White JH. Ligand-dependent nuclear receptor corepressor lcor functions by histone deacetylase-dependent and -independent mechanisms. *Mol. Cell*. 2003;11:139-150. doi: 10.1016/S1097-2765(03)00014-5.
40. Reilly SM, Bhargava P, Liu S, Gangl MR, Gorgun C, Nofsinger RR, Evans RM, Qi L, Hu FB, Lee CH. Nuclear receptor corepressor smrt regulates mitochondrial oxidative metabolism and mediates aging-related metabolic deterioration. *Cell Metab.* 2010;12:643-653. doi: 10.1016/j.cmet.2010.11.007.
41. Mills EL, Kelly B, O'Neill LAJ. Mitochondria are the powerhouses of immunity. *Nat. Immunol.* 2017;18:488-498. doi: 10.1038/ni.3704.

42. Schneider JG, Yang Z, Chakravarthy MV, Lodhi IJ, Wei X, Turk J, Semenkovich CF. Macrophage fatty-acid synthase deficiency decreases diet-induced atherosclerosis. *J. Biol. Chem.* 2010;285:23398-23409. doi: 10.1074/jbc.M110.100321.
43. Hartmann P, Zhou Z, Natarelli L, Wei Y, Nazari-Jahantigh M, Zhu M, Grommes J, Steffens S, Weber C, Schober A. Endothelial dicer promotes atherosclerosis and vascular inflammation by mirna-103-mediated suppression of klf4. *Nat. Commun*. 2016;7:10521. doi: 10.1038/ncomms10521.
44. Feingold KR, Wang Y, Moser A, Shigenaga JK, Grunfeld C. Lps decreases fatty acid oxidation and nuclear hormone receptors in the kidney. *J. Lipid Res.* 2008;49:2179-2187. doi: 10.1194/jlr.M800233-JLR200.
45. Hayashida S, Arimoto A, Kuramoto Y, Kozako T, Honda S, Shimeno H, Soeda S. Fasting promotes the expression of sirt1, an nad+ -dependent protein deacetylase, via activation of pparalpha in mice. *Mol. Cell Biochem.* 2010;339:285-292. doi: 10.1007/s11010-010-0391-z.
46. Kersten S. Integrated physiology and systems biology of pparalpha. *Mol. Metab*. 2014;3:354-371. doi: 10.1016/j.molmet.2014.02.002.
47. Calderon MR, Verway M, An BS, DiFeo A, Bismar TA, Ann DK, Martignetti JA, Shalom-Barak T, White JH. Ligand-dependent corepressor (lcor) recruitment by kruppel-like factor 6 (klf6) regulates expression of the cyclin-dependent kinase inhibitor cdkn1a gene. *J. Biol. Chem*. 2012;287:8662-8674. doi: 10.1074/jbc.M111.311605.
48. Chae S, Ahn BY, Byun K, Cho YM, Yu MH, Lee B, Hwang D, Park KS. A systems approach for decoding mitochondrial retrograde signaling pathways. *Sci. Signal*. 2013;6:rs4. doi: 10.1126/scisignal.2003266.
49. Foley NH, Bray I, Watters KM, Das S, Bryan K, Bernas T, Prehn JH, Stallings RL. Micrornas 10a and 10b are potent inducers of neuroblastoma cell differentiation through targeting of nuclear receptor corepressor 2. *Cell Death Differ*. 2011;18:1089-1098. doi: 10.1038/cdd.2010.172.
50. Njock MS, Cheng HS, Dang LT, Nazari-Jahantigh M, Lau AC, Boudreau E, Roufaiel M, Cybulsky MI, Schober A, Fish JE. Endothelial cells suppress monocyte activation through secretion of extracellular vesicles containing antiinflammatory micrornas. *Blood*. 2015;125:3202-3212. doi: 10.1182/blood-2014-11-611046.

Figure Legends

Figure 1. *Dicer* deficiency exacerbates atherosclerosis in *Apoe*$^{-/-}$ mice. *M-Dicer*$^{+/+}$ or *M-Dicer*$^{-/-}$ mice were fed the HFD for 12 weeks. **A,** Lesion formation in Oil red O-stained, *en face* prepared aortas. *n* = 13 or 14 mice per group. **B,** Lesion formation and necrotic core area in aortic roots quantified in sections stained with Elastic van Gieson stain. Scale bars, 200 μm. *n* = 8 or 9 mice per group. **C,** The percentage of lipid-droplets containing (PLIN2^{+}) macrophages in lesional macrophages quantified by double immunostaining of PLIN2 (green) and MAC2 (red) in aortic roots. Scale bars, 20 μm. *n* = 8 mice per group. # indicates the lumen. **D,** The percentage of macrophages undergoing cell death (Caspase3^{+}) within the lesion quantified by double immunostaining of cleaved Caspase3 (green) and MAC2 (red) in aortic roots. Arrows indicate the Caspase3^{+} macrophages. Scale bars, 20 μm. *n* = 8 mice per group. # indicates the lumen. **E,** Transcript levels of inflammatory mediators and AAM markers in atherosclerotic lesions collected via laser capture microdissection from aortic arch. *n* = 4–6 mice per group. All data are represented as mean ± SEM. **P* < 0.05 by Student's t test.

Figure 2. Dicer promotes alternative macrophage activation by enhancing mitochondrial oxidative metabolism. **A,** Relative mRNA levels of pro-inflammatory mediators and AAM markers in *Dicer*$^{+/+}$ and *Dicer*$^{-/-}$ BMDMs treated as indicated. *n* = 3. **B,** Downregulated and top 4 upregulated ingenuity canonical pathways (absolute z-score > 2, *P* < 0.05) in resting *Dicer*$^{-/-}$ BMDMs compared with *Dicer*$^{+/+}$ BMDMs. *n* = 3. PRR, pattern recognition receptor. **C,** OCR of vehicle-, IL-4- or LPS/IFN-γ-stimulated *Dicer*$^{+/+}$ and *Dicer*$^{-/-}$ BMDMs at basal condition and after the sequential treatment with oligomycin (Oligo), FCCP and rotenone/antimycin (Rot+Ant).

n = 3 or 5. **D–F,** Basal OCR (**D**), ATP production (**E**) and relative cell death rate (**F**) in *Dicer*$^{+/+}$ and *Dicer*$^{-/-}$ BMDMs treated as indicated. *n* = 3–5. eto, etomoxir. The data in (**F**) are normalized to the IL-4-treated *Dicer*$^{+/+}$ group. **G,** Relative mRNA levels of genes related to mitochondrial oxidative metabolism in IL-4-stimulated *Dicer*$^{+/+}$ and *Dicer*$^{-/-}$ BMDMs. *n* = 3. FAO, fatty acid oxidation; TCA, tricarboxylic acid cycle; ETC, electron transport chain. **H,** Histograms of flow cytometric analysis of MitoTracker Green staining in *Dicer*$^{+/+}$ (WT) or *Dicer*$^{-/-}$ (KO) BMDMs with or without IL-4 treatment. **I,** Contour plots of flow cytometric analysis of double staining with MitoTracker Green and MitoTracker Deep Red in IL-4-treated *Dicer*$^{+/+}$ or *Dicer*$^{-/-}$ BMDMs. *n* = 5. The data in A, C–G, and I are represented as mean ± SEM. **P* < 0.05, ***P* < 0.005 and ****P* < 0.001 by Student's t test (A, C, G and I), one-way ANOVA followed by Fisher's LSD test (F) and two-way ANOVA followed by Tukey-Kramer test (D, E).

Figure 3. Dicer limits foam cell formation by promoting mitochondrial oxidative metabolism. *Dicer*$^{+/+}$ or *Dicer*$^{-/-}$ BMDMs were treated with vehicle, nLDL or oxLDL for 72 h. **A,** OCR of vehicle-, nLDL- or oxLDL-treated *Dicer*$^{+/+}$ BMDMs at basal condition and after the sequential treatment with Oligo, FCCP and Rot+Ant. *n* = 5, **P* < 0.05 and ***P* < 0.005 *versus* vehicle and nLDL. **B,** Relative mRNA levels of genes related to mitochondrial oxidative metabolism in vehicle-, nLDL- or oxLDL-treated *Dicer*$^{+/+}$ BMDMs. *n* = 3 or 4. **C,** Relative mRNA levels of *Tnf*, *Fizz1* and *Ym1* in *Dicer*$^{+/+}$ and *Dicer*$^{-/-}$ BMDMs treated with nLDL or oxLDL. *n* = 3–5. **D,** OCR of oxLDL-treated *Dicer*$^{+/+}$ and *Dicer*$^{-/-}$ BMDMs at basal condition and after the sequential treatment with Oligo, FCCP and Rot+Ant. *n* = 5. **E,** Relative mRNA levels of genes related to mitochondrial oxidative metabolism in *Dicer*$^{+/+}$ and *Dicer*$^{-/-}$ BMDMs treated with oxLDL. *n* = 4–6. **F,** Lipid deposition in oxLDL-treated *Dicer*$^{+/+}$ and *Dicer*$^{-/-}$ BMDMs in the absence or

presence of etomoxir determined by Oil red O staining. Scale bars: 50 μm. *n* = 3 or 4. **G,** Basal OCR of oxLDL-treated *Dicer*$^{+/+}$ BMDMs in the absence or presence of etomoxir. *n* = 4 or 5. All data are represented as mean ± SEM. **P* < 0.05, ***P* < 0.005 and ****P* < 0.001 by Student's t test (D, E and G), one-way ANOVA followed by Fisher's LSD (A, B) or Tukey-Kramer (C) test and two-way ANOVA followed by Tukey-Kramer test (F). Oligo, oligomycin; Rot, rotenone; Ant, antimycin; TCA, tricarboxylic acid cycle; ETC, electron transport chain.

Figure 4. Repressing Lcor and Ncor2 Mediates *Dicer* Effects on Mitochondrial Function in AAMs. **A,** miRNA profiles in *Dicer*$^{-/-}$ BMDMs compared with *Dicer*$^{+/+}$ BMDMs. Downregulated miRNAs (*P* < 0.05) are labeled in red. *n* = 3. **B,** Predicted interactions between downregulated miRNAs and upregulated mRNAs in *Dicer*$^{-/-}$ BMDMs. The rectangle size indicates the fold change (FC > 2) of mRNA expression in *Dicer*$^{-/-}$ *versus Dicer*$^{+/+}$ BMDMs; the rectangle color indicates the FC (> 2) of mRNA enrichment in AGO2-complexes of *Dicer*$^{+/+}$ *versus Dicer*$^{-/-}$ BMDMs. miRNAs are shown as diamonds: the light blue diamonds indicate the miRNAs predicted to target Lcor. The black and pink lines indicate Lcor-miRNA and Ncor2-miRNA interactions, respectively. The line thickness represents the probability of conserved targeting (P_{CT}) values that are used to assess biological relevance for predicted miRNA-mRNA interaction by TargetScan. **C,** Enrichment of *Lcor* and *Ncor2* in AGO2-immunoprecipitated RNAs in *Dicer*$^{+/+}$ and *Dicer*$^{-/-}$ BMDMs quantified by qRT-PCR. **D–F,** Relative mRNA levels of *Lcor* and *Ncor2* in *Dicer*$^{+/+}$ and *Dicer*$^{-/-}$ BMDMs treated with IL-4 (**D**; *n* = 3) or oxLDL (**E**; *n* = 3 or 5), and in aortic arch lesions of *M-Dicer*$^{+/+}$ and *M-Dicer*$^{-/-}$ mice after 12-week HFD period (**F**; *n* = 4 or 5). **G–I,** OCR (**G**; *n* = 3 or 4), relative gene expression (**H;** *n* = 4 or 5) and non-respiring mitochondria ratio (**I;** *n* = 4) in *Dicer*$^{-/-}$ AAMs transfected with *Lcor*, *Ncor2* or control

GapmeRs. **J,** Relative luciferase activity in HEK293T cells co-transfected with reporters containing RXR transcriptional response elements along with RXRα overexpression, Lcor overexpression or control (vec) vectors in the presence of 9-cis-retinoic acid. *n* = 3–5. **K,** Relative mRNA levels of *Fizz1* and *Ym1* in *Dicer*$^{-/-}$ AAMs treated with or without CD3254. *n* = 3–5. The data in D–K are represented as mean ± SEM. **P* < 0.05, ***P* < 0.005 and ****P* < 0.001 by Student's t test (E–G and K), one-way ANOVA followed by Fisher's LSD (H–J) or Tukey-Kramer (D) test.

Figure 5. Lcor-Targeting miRNAs, miR-10a and let-7b Contribute to the Effect of Dicer in Macrophages. **A,** OCR of *Dicer*$^{-/-}$ and *Dicer*$^{+/+}$ AAMs transfected with miR-10a, let-7b, miR-195a or control mimics. *n* = 3 or 4. **P* < 0.05 blue *versus* red or black, $^{\#}$*P* < 0.05 red *versus* blue, §*P* < 0.05 black *versus* blue or red; ¶*P* < 0.05 among all three groups and $^{\infty}$*P* < 0.05 black *versus* blue. **B** and **C,** Relative luciferase activity in HEK293T cells co-transfected with mimics of miR-10a (**B**) or let-7b (**C**) and the psiCHECK2 vectors containing *Lcor* 3′-UTR without (*Lcor*) or with mutated binding site of miR-10a (mut*Lcor*-10a) or let-7b (mut*Lcor*-let7b), or *Ncor2* 3′-UTR without (*Ncor2*) or with mutated binding site of miR-10a (mut*Ncor2*-10a). *n* = 5 or 6. **D** and **E**, Relative mRNA levels of *Ncor2* and/or *Lcor* in *Dicer*$^{-/-}$ AAMs transfected with miR-10a, let-7b, miR-195a or control mimics (**D**; *n* = 4 or 5), and in *Dicer*$^{+/+}$ AAMs transfected with miR-10a, let-7b, miR-195a or control inhibitors (inh) (**E**; *n* = 3–5). **F,** Expression pattern of miR-10a and let-7b in aortic root lesions from *M-Dicer*$^{+/+}$ and *M-Dicer*$^{-/-}$ mice after 12-week HFD feeding period determined by combined *in situ* PCR and MAC2 immunostaining. # indicates the lumen. Scale bars: 25 μm. **G** and **H,** Expression levels of miR-10a and let-7b in the aortas from *M-Dicer*$^{+/+}$ and *M-Dicer*$^{-/-}$ mice fed the HFD for 12 weeks (**G**), and in human vessel walls (control)

and carotid plaques macroscopically dissected from the same atherosclerotic artery (**H**). *n* = 3. **I,** Correlation of miR-10a and let-7b expression with necrotic core area in human carotid lesions. *n* = 23. The data in A–E and G–H are represented as mean ± SEM. **P* < 0.05, ***P* < 0.005 and ****P* < 0.001 by Student's t test (B–E and G–H) and one-way ANOVA followed by Tukey-Kramer test (A). ctrl, control.

Figure 6. The effect of miR-10a on macrophages is mediated by targeting of Lcor and Ncor2. **A–E,** Relative mRNA levels of *Sirt1*, *Ppargc1b*, *Mrc1*, *Fizz1* and *Ym1* in IL4-stimulated *M-Dicer*$^{+/+}$ BMDMs transfected with miR-10a inhibitor (inh) (**A**), let-7b inhibitor (**B**), miR10a/*Lcor* TSB (**C**), miR10a/*Ncor2* TSB (**D**), let7b/*Lcor* TSB (**E**) or scrambled control (ctrl). *n* = 3–5. **F**, Relative mRNA levels of *Sirt1*, *Ppargc1b*, *Mrc1*, *Fizz1* and *Ym1* in IL-4-stimulated *Dicer*$^{+/+}$ BMDMs transfected with TSBs in the presence of CD3254. *n* = 5 or 6. **G,** Basal OCR of IL-4-treated *Dicer*$^{+/+}$ BMDMs transfected with TSBs. *n* = 3 or 4. **H,** Cell death rate of IL-4-treated *Dicer*$^{+/+}$ BMDMs transfected with TSBs determined by flow cytometric analysis after Annexin V and PI staining. *n* = 3–5. **I–K,** Basal OCR (**I**; *n* = 3 or 4), relative mRNA levels of *Sirt1* and *Ppargc1b* (**J**; *n* = 4 or 5) and Oil red O staining (**K**; scale bars, 25 μm) in oxLDL-treated *Dicer*$^{+/+}$ BMDMs transfected with miR10a/*Lcor*, miR10a/*Ncor2* or control TSBs. **L** and **M,** Lesion formation in Oil red O-stained, *en face* prepared aortic arches (**L**; *n* = 6 or 7), and relative expression of *Lcor*, *Sirt1*, *Ppargc1b*, AAM and inflammatory markers in thoracic aortas (**M**; *n* = 5–7) from *Apoe*$^{-/-}$ mice treated with control (ctrl) or miR10a/*Lcor* TSBs during 12-week HFD feeding program. All data except K are represented as mean ± SEM. **P* < 0.05, ***P* < 0.005 and ***P < 0.001 by Student's t test (A–E, I, J, L and M) and one-way ANOVA followed by Fisher's LSD test (F–H).

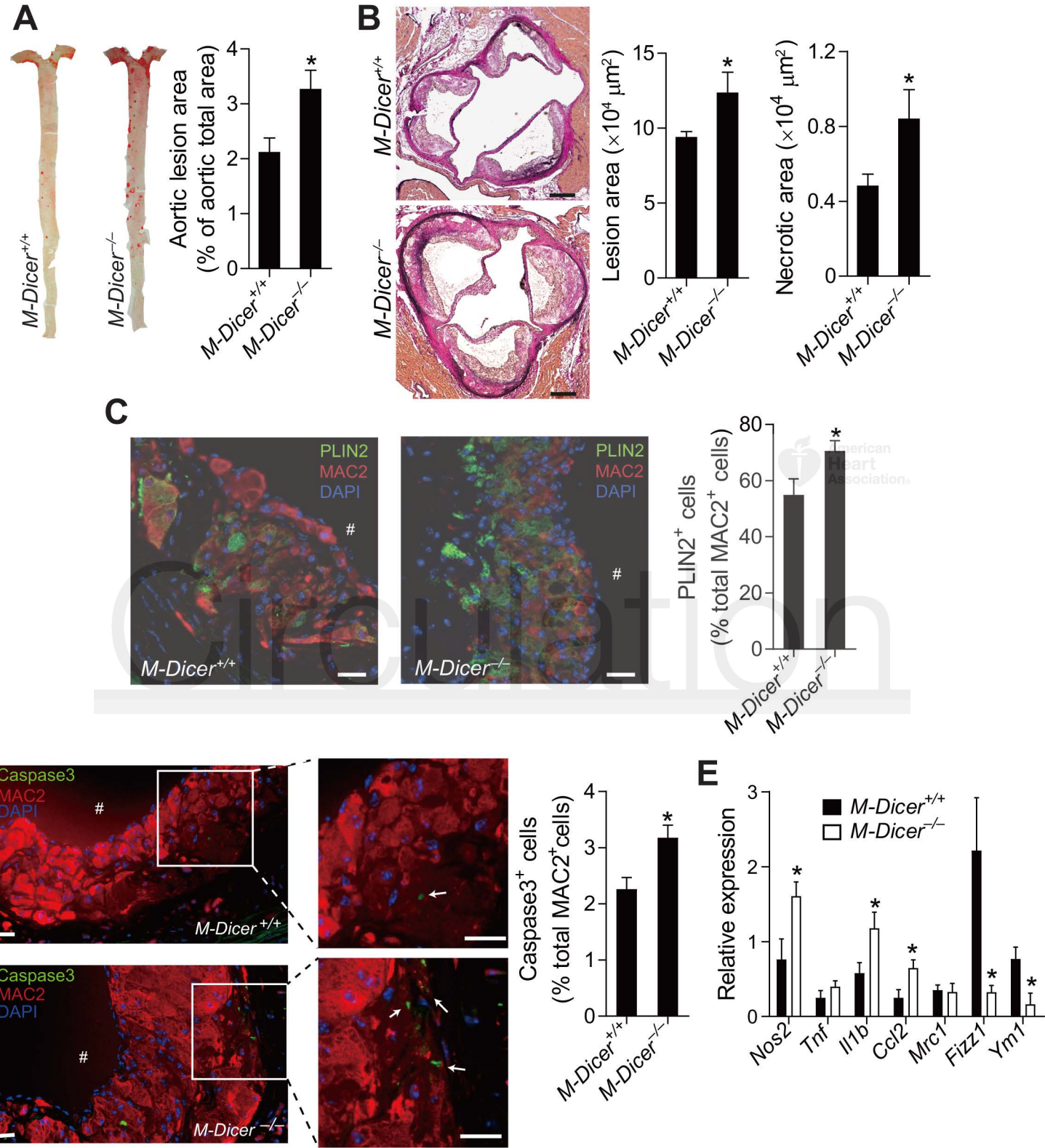

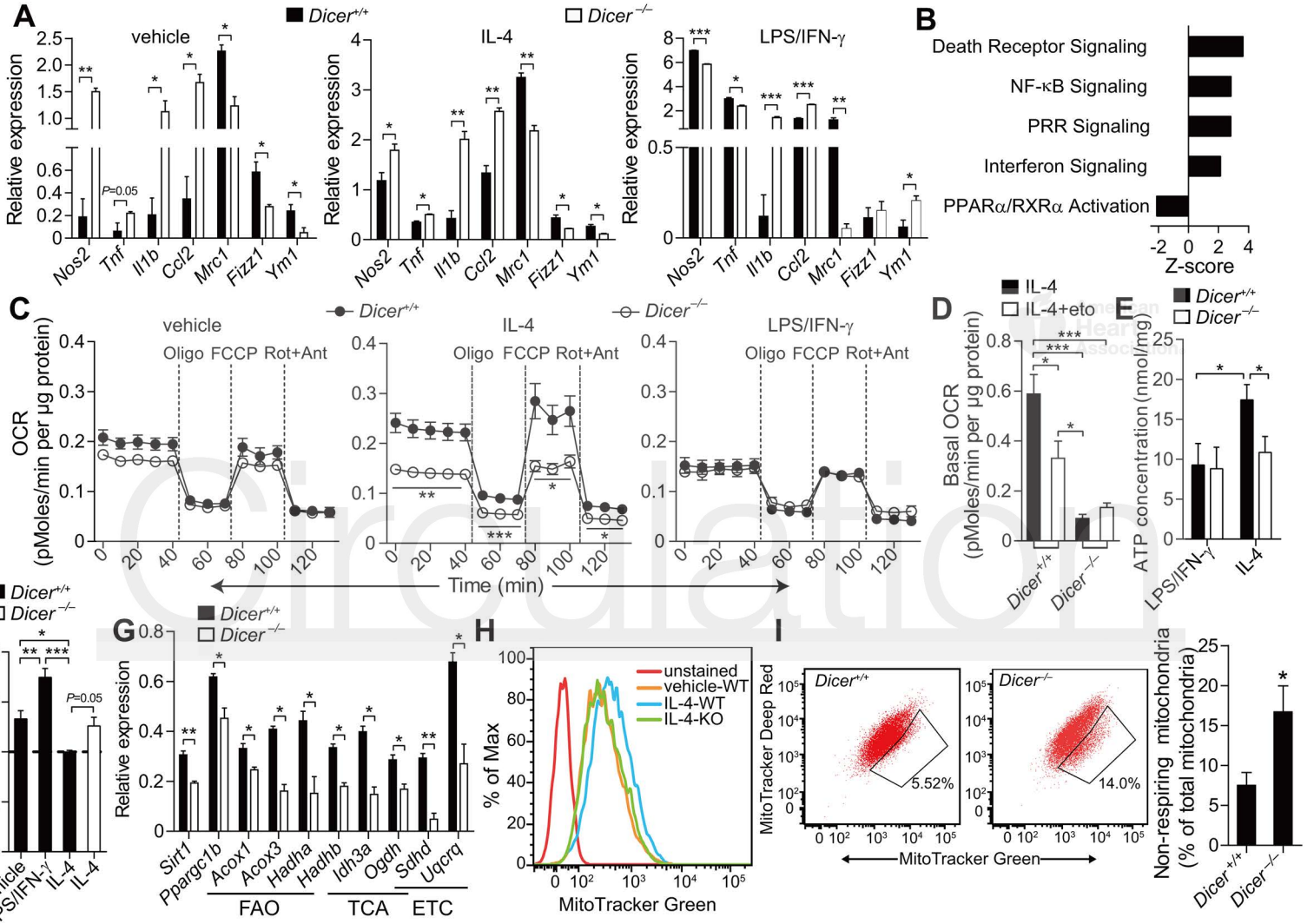

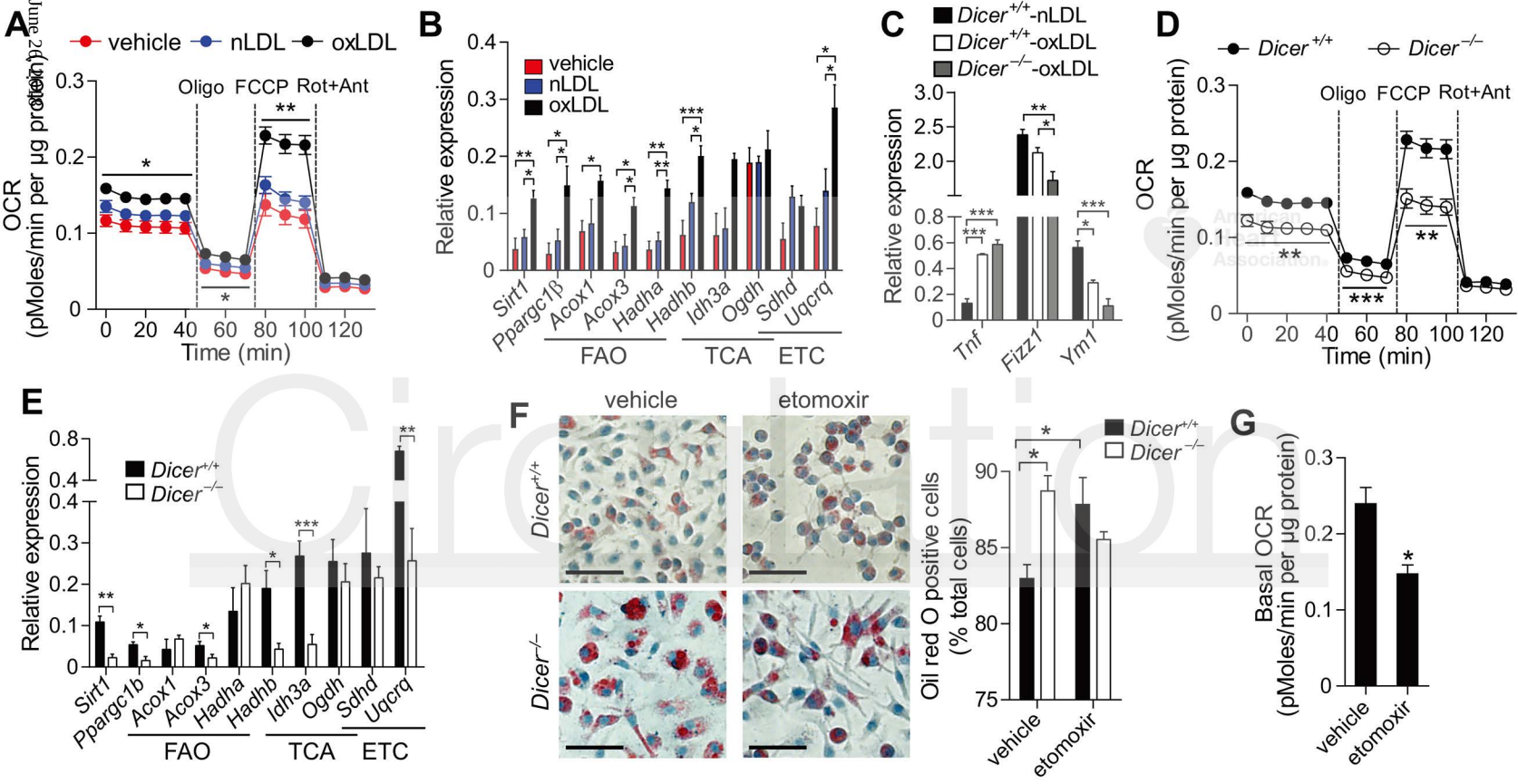
A
vehicle
nLDL
oxLDL
OCR (pMoles/min per µg protein)
Oligo
FCCP
Rot+Ant
Time (min)
B
vehicle
nLDL
oxLDL
Relative expression
Sirt1
Ppargc1β
Acox1
Acox3
Hadha
Hadhb
Idh3a
Ogdh
Sdhd
Uqcrq
FAO
TCA
ETC
C
Dicer+/+-nLDL
Dicer+/+-oxLDL
Dicer−/−-oxLDL
Relative expression
Tnf
Fizz1
Ym1
D
Dicer+/+
Dicer−/−
OCR (pMoles/min per µg protein)
Oligo
FCCP
Rot+Ant
Time (min)
E
Dicer+/+
Dicer−/−
Relative expression
Sirt1
Ppargc1b
Acox1
Acox3
Hadha
Hadhb
Idh3a
Ogdh
Sdhd
Uqcrq
FAO
TCA
ETC
F
vehicle
etomoxir
Dicer+/+
Dicer−/−
Oil red O positive cells (% total cells)
vehicle
etomoxir
G
Basal OCR (pMoles/min per µg protein)
vehicle
etomoxir

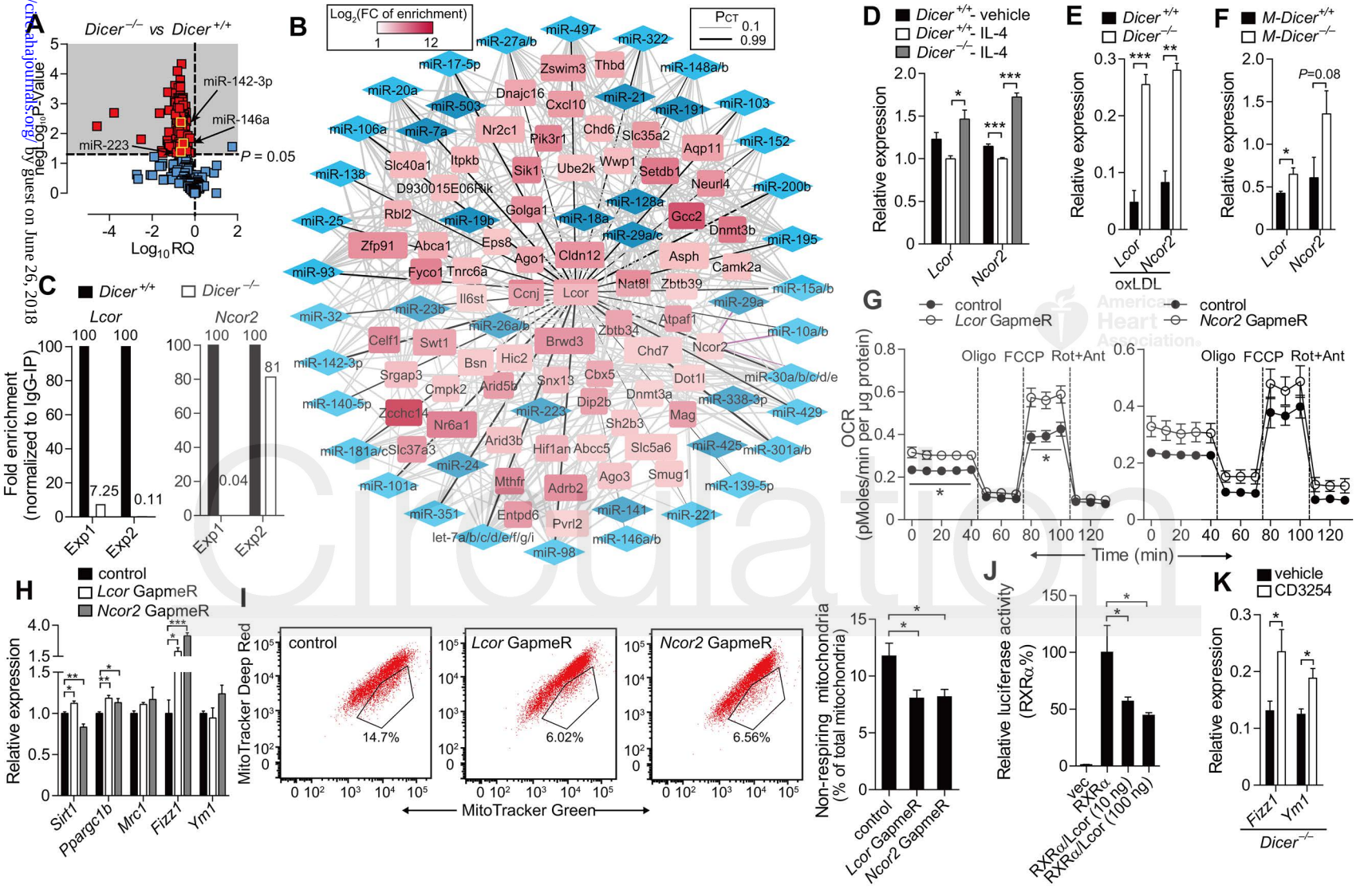

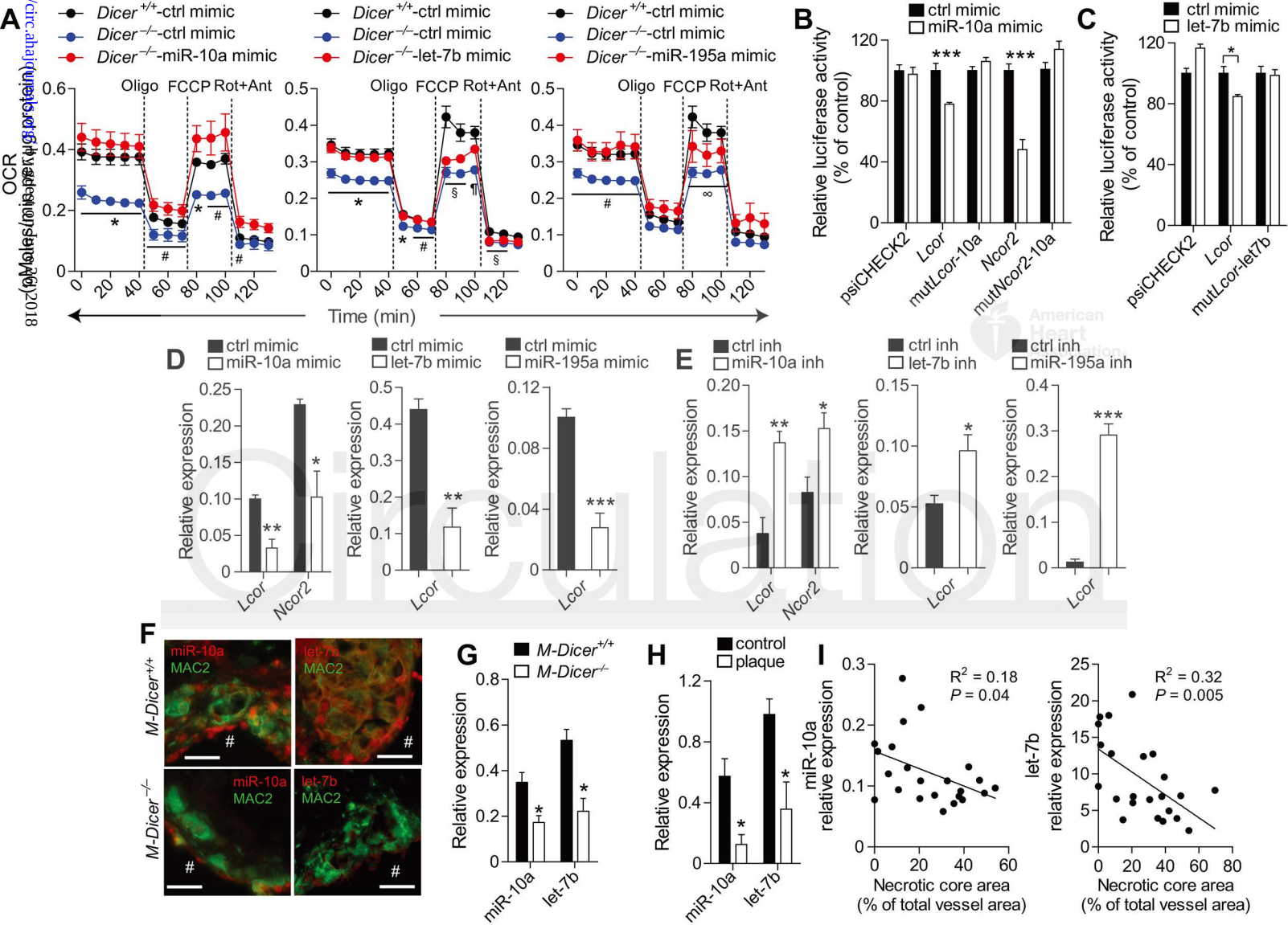

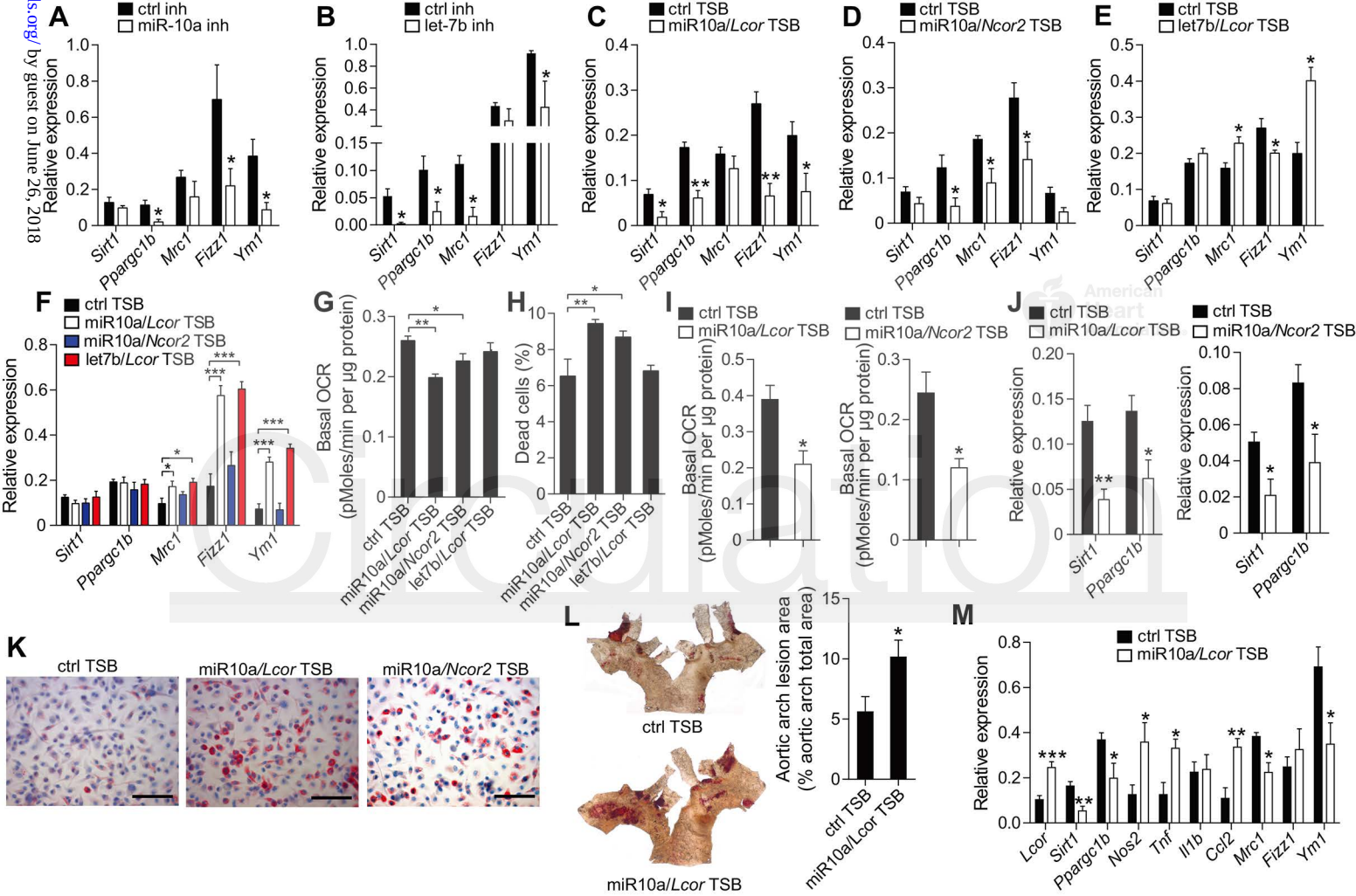

Dicer in Macrophages Prevents Atherosclerosis by Promoting Mitochondrial Oxidative Metabolism

Yuanyuan Wei, Judit Corbalán-Campos, Rashmi Gurung, Lucia Natarelli, Mengyu Zhu, Nicole Exner, Florian Erhard, Franziska Greulich, Claudia Geißler, N. Henriette Uhlenhaut, Ralf Zimmer and Andreas Schober

Circulation. published online May 10, 2018;
Circulation is published by the American Heart Association, 7272 Greenville Avenue, Dallas, TX 75231

Print ISSN: 0009-7322. Online ISSN: 1524-4539

SUPPLEMENTAL MATERIAL

Supplemental Methods

Mice

To generate Apoe$^{-/-}$ mice containing a loxP site-flanked Dicer sequence[1] and a transgene with Cre recombinase under the control of the myeloid cell-specific M–lysozyme (LysM) promoter, *LysM^{Cre}* mice were crossed with *Dicer$^{flox/flox}$/Apoe$^{-/-}$* mice (The Jackson Laboratory) to obtain *LysM^{Cre}/Dicer$^{WT/flox}$/Apoe$^{-/-}$* mice. The deletion allele was genotyped in bone marrow derived-macrophages (BMDMs) by using primers 5′-CCTGACAGTGACGGTCCAAAG and 5′-CCTGAGCAAGGCAAGTCATTC. The deletion allele produced a 471-bp PCR product whereas a wild-type allele resulted in a 1,300-bp product.

Blood cell differentiation count and cholesterol measurement

Mice were anesthetized with ketamine (80 mg/kg) and medetomidine (0.3 mg/kg). Blood was retro-orbitally collected into EDTA- and Z-gel-coated tubes for cell counts and serum separation, respectively. Cell counts were determined using an automated hematology analyzer (scil Animal Care). Serum samples were analyzed by dry chemistry using a Vitros 250 Analyzer (Ortho Clinical Diagnostics) to determine the levels of cholesterol.

Histology and immunostaining

After overnight fixation and adventitia removal, the aorta was longitudinally opened and stained en face with Oil Red O to visualize the lipid deposition. Serial sections (4 μm thick) of aortic roots (5 sections per mouse) were stained with Elastic van Gieson stain. Images were obtained with a bright-field microscope (Leica, DM6000B) connected to a CCD camera. The lesion and the necrotic core area, which was defined as the lipid-rich, acellular region within the lesion, were quantified using image analysis software (ImageJ)[2]. The immunostaining of SMA (M0851, Dako), MAC2 (CL8942AP, Cederlane), Cleaved Caspase3 (9661S, Cell Signaling), PLIN2 (NB110-40877, Novus Biologicals), LCoR (ab48339, Abcam) and NCoR2 (ab5802, Abcam) were performed. Non-specific primary antibodies were used as negative controls. The primary antibodies were detected with a fluorescently labelled secondary antibody. Digital images were acquired with a fluorescence microscope (Leica, DM6000B) that was connected to a CCD camera and LAS software. The size of the positively stained

area or the number of the positively stained cells per lesion area (2-3 sections per mouse) were determined with ImageJ, and the threshold was set according to the background of the negative control staining.

Laser capture microdissection

The aortic arch were harvested from *M-Dicer*$^{+/+}$ and *M-Dicer*$^{-/-}$ mice after a 12-week HFD feeding period, fixed using the PAXgene tissue containers (Qiagen) and embedded in paraffin. Serial sections (8 μm thick) were mounted on polyester-membrane frame slides (Leica), deparaffinized under RNase-free conditions, and completely dried. Lesions excluding endothelium were collected using a laser microdissection system (LMD7000, Leica). RNA was isolated with the PAXgene Tissue miRNA Kit (Qiagen) and followed by the reverse transcription and pre-amplification with Ovation PicoSL WTA System V2 (NuGEN).

Cell culture

Bone marrow-derived cells from the femurs of *M-Dicer*$^{+/+}$ or *M-Dicer*$^{-/-}$ mice were harvested and cultured in DMEM/F12 supplemented with 10% FBS and 10% L929-conditioned medium, as previously described[3]. After 7 days of culture, the macrophages were stimulated with either IL-4 (5 ng/ml for 16 h; PeproTech) or LPS (100 ng/ml for 24 h; Sigma-Aldrich) and interferon gamma (IFN-γ, 10 ng/ml for 16 h; PeproTech). In some experiments, the macrophages were treated with CD3254 (10 μM; Torics Bioscience) 8 h prior to IL-4 treatment.

To generate oxidized low-density lipoprotein (oxLDL), human low-density lipoproteins (Merck) were dialysed using D-tube Midi Dialyzer tubes (Merck) and incubated with 10 μM $CuSO_4$ at 37 °C. The reaction was stopped by adding 20 μM EDTA when the absorbance at 234 nm was not changed in 1 h measured using Nano Drop. After passing PD-10 desalting column (GE Healthcare), the oxLDL was stored at 4 °C and was used in one week. The macrophages were pre-treated with or without etomoxir (100 μM; Sigma-Aldrich) for 1 h followed by the treatment with native LDL or oxLDL (100 μg/ml) for 72 h. To visualize the lipid accumulation, the cells were fixed with 4% paraformaldehyde, and then stained with Oil red O.

miRNA real-time PCR array

Total RNA was reverse-transcribed and pre-amplified (Megaplex RT & Preamp Primers, Rodent Pool Set, Thermo Fisher Scientific) according to the manufacturer's instructions. The samples were loaded onto preconfigured 384-well microfluidic cards (TaqMan Array Rodent microRNA Cards v3.0, Thermo Fisher Scientific) for the real-time analysis. The data were analyzed with qbase software (Biogazelle) according to the $\Delta\Delta$Ct method, with multiple internal control genes. The miRNAs with Ct value > 35 in at least two wild-type samples were defined as the ones that are not expressed in murine macrophages.

Western blot

Efficiency of AGO2-immunoprecipitation, as well as the knockdown efficiency of *Lcor* and *Ncor2* GapmeRs at protein levels was assessed by Western blot. Total proteins extracted in RIPA buffer or the cell lysates collected before and after AGO2 or IgG immunoprecipitation were eluted in SDS-PAGE loading buffer containing β-mercaptoethanol. For LCoR and AGO2 protein detection, 20 µg of proteins were resolved using SDS/Mini-PROTEAN TGX Precast gels of 4-15% range (Bio-Rad) and blotted on 0.45 µm nitrocellulose (for AGO2) or 0.2 µm (for LCoR) polyvinylidene fluoride (PVDF) membranes, blocked for 1 hour in 10% PBST-diluted milk (0.1% Tween-20 in PBS). Membranes were incubated with anti-EIF2C2 (H00027161-M01, Abnova) or anti-LCoR antibody (ab48339, Abcam) at 0.5 µg/ml dilution in PBST 5% milk at 4°C overnight. For NCoR2 protein detection, 20 µg of proteins were resolved using a 4% Tris-glycine SDS-polyacrylamide gel and blotted on 0.45 µm nitrocellulose membrane blocked for 1 hour in 10% PBST-diluted milk. Nitrocellulose membrane was incubated at 4°C overnight with anti-Ncor2 antibody (ab5802, Abcam. 4 µg/ml dilution in PBST 5% milk). Membranes were washed three times in PBST and incubated with HRP-conjugated secondary antibody. After three additional washes with PBST, proteins were detected using SuperSignal West Pico Chemiluminescent Substrate (Thermo Fisher Scientific), followed by analysis with the CCD camera detection system Las4000 Image Quant (GE Healthcare). Lamin B was used as housekeeping and quality

control for NCoR2, β-tubulin was used as housekeeping and quality control for AGO2 and LCoR.

Metabolism assays

For real-time analysis of extracellular acidification rate (ECAR) and oxygen consumption rate (OCR), BMDMs were analyzed with an XF-96 Extracellular Flux Analyzer (Seahorse Bioscience). Three or more consecutive measurements were obtained under basal conditions and after the sequential addition of 1 μM oligomycin, 1 μM fluoro-carbonyl cyanide phenylhydrazone (FCCP), and 1 μM rotenone plus 1 μM antimycin A (all drugs for this assay from Sigma-Aldrich). To study the oxygen consumption derived from fatty acid oxidation, the macrophages were treated with etomoxir (40 μM) for 15 min at 37 °C prior to the assay.

Luciferase assay

The full-length 3′-UTR of murine *Lcor* and *Ncor2* were cloned into the psiCHECK-2 Vector (Promega) at the XhoI/NotI sites. Mutagenesis PCR at the miR-10a target sites of *Lcor* and *Ncor2* was performed with the following sets of primers: *Lcor* mutagenic primers: 5′-TTACTCAGGAGCAGTCTCCCTACATTTCATAA and 5′-GGGAGACTGCTCCTGAGTAAGAAGGGAGCGGG; *Ncor2* mutagenic primers: 5′-AATGGTGTTGGCTTACTCCCTATATTTTTGAT and 5′-GGGAGTAAGCCAACACCATTTAC ACGTGCCTT. Mutagenesis PCR at the let-7b target site of *Lcor* was performed with the following sets of primers: 5′-CACAGAGAATTGAGTTTGGACACAAAGACCAG and 5′-TCCAAACTCAATTCTCTGTGTAGAGAAACATG. HEK293 cells were cultured in 96-well plate until subconfluency and co-transfected with 100 ng of luciferase reporter or empty vector and miR-10a, let-7b mimics or scrambled control (30 nM, Thermo Fisher Scientific) using Lipofectamine 2000 (Thermo Fisher Scientific).

For RXRα reporter assay, murine Lcor coding sequence was subcloned into pCMV-tag2b vector. HEK293 cells were cultured in 96-well plate and transfected with Cignal RXR reporter (100 ng; Qiagen) in the absence or presence of RXRα expression vectors (100 ng; MC216284, OriGene Technologies) combined with or without the Lcor expression vectors

(10 ng or 100 ng). 24 h after the transfection, the cells were stimulated with 9c-RA (Santa Cruz Biotechnology).

The Firefly and Renilla luciferase activities were measured with the Dual-Glo Luciferase Assay System (Promega) using a microplate reader (Tecan) 48 h after transfection.

Flow Cytometric Analyses

Mitochondrial mass was measured by fluorescence levels upon staining with MitoTrackerGreen (to stain total mitochondria) and MitoTracker Deep Red (to stain respiring mitochondria) (Thermo Fisher Scientific) at 100 nM for 25 min at 37 °C. Cells were then washed with PBS solution, detached using Accutase (Sigma-Aldrich) and resuspended in PBS solution containing1% FBS for FACS analysis. Dysfunctional non-respiring mitochondria were defined as MitoTrackerGreen-positive and MitoTracker Deep Red-negative. To measure the cell death rate, macrophages were stained with Annexin V-FITC/PI Apoptosis Detection Kit (eBioscience) according to the manufacturer's instructions. Samples were measured by flow cytometry (FACSCanto II, BD Biosciences) after appropriate compensation settings and analyzed by FlowJo v.10 software (Tree Star Inc.).

Mitochondrial DNA Quantification

Relative mitochondrial DNA amount was assessed by quantitative PCR of mitochondrial 16s rRNA and normalized to nuclear hexokinase 2 level in total DNA from the BMDMs isolated using the DNeasy Blood & Tissue kit (Qiagen). The primers are listed in Supplementary Table 2.

ATP measurement

Cellular ATP production was measured using ATP determination kit (Thermo Fisher Scientific) according to the manufacturer's instructions.

***In situ* PCR**

In situ PCRs of miR-10a and let-7b were followed according to previous publication with small modification[4]. In brief, sections (4 μm in thickness) from PAXgene-fixed and paraffin-embedded aortic roots were cooked in citrate buffer and treated with DNase I (Roche) after deparaffinization. After DNase digestion, the tissue section was covered with the PCR

solution consisted of primers, digoxigenin dUTP (Roche), RNase inhibitor (Roche) and SuperScript One-Step RT-PCR System with Platinum Taq DNA Polymerase (Thermo Fisher Scientific). For miR-10a *in situ* PCR, the sections were incubated in the PCR solution (primer sequence: 5′-GACCCCTTAATGCGTCTAAAGACCCCTTAATGCGTCTAAAGACCCCTTAATGCGTCTAAACACAAATTCGGATCTACAGGGTA) for 35 min at 52 °C. For let-7b *in situ* PCR, the sections were incubated in the PCR solution (primer1: 5′-GTCGTATCCAGTGCAGGGTCCGAGGTATTCGCACTGGATACGACAACCAC; primer2: 5′-GCCGCTGAGGTAGTAGGTTGTG; primer3: 5′-GTGCAGGGTCCGAGGT) for 30 min at 50 °C followed by a PCR cycle. The scrambled primer was used as negative control. The digoxigenin-labeled miRNA cDNA or amplicon was detected with digoxigenin antibody (Roche) followed by MAC2 staining.

Statistical analysis

Sample size (number of mice) was determined on the basis of our previous studies[3, 5, 6]. Mice were randomized to experimental groups in TSB-injected experiment using a random number table. For most mouse experiments, the investigators were blinded when assessing the results without knowing the group. In some cases, selected samples were excluded from specific analyses because of technical flaws during sample processing or data acquisition.

Supplemental Tables

Supplemental Table 1. Sequences of miRNA inhibitors, GapmeRs and TSBs.

Oligonucleotide names	Sequences (5′ → 3′)
miR-10a inhibitor	ACAAATTCGGATCTACAGGGT
let-7b inhibitor	ACCACACAACCTACTACCTC
miR-195a inhibitor	CCAATATTTCTGTGCTGCT
Lcor GapmeR	AGGATGCCATGAGAAT
Ncor2 GapmeR	GCAAGGCGGTCGATGG
miR10a/*Lcor* TSB	TACCCTGACTGCTCCT
miR10a/*Ncor2* TSB	TACCCTGTAAGCCAAC
let7b/*Lcor* TSB	GAGGTAACTCAATTCT
Scramble control TSB	ACGTCTATACGCCCA

Supplemental Table 2. Primer sequences for qRT-PCRs.

Gene	Primer sequences (5′ → 3′)	Gene	Primer sequences (5′ → 3′)
Dicer	F: GAATAAGGCTTATCTTCTGCAGG	*Hadhb*	F: AAGCCTTCTCAGGCCAGATTT
	R: CATAAAGGTGCTTGGTTATGAGG		R: CCAGAGACAGTGATCCGCC
Nos2	F: TCATTGGGCCTGGTACGGGCA	*Idh3a*	F: GGGAAGTTGCGGAGAACTGTA
	R: ACACCAAGCTCATGCGGCCTC		R: AGTCCTGCACACAGATCACTAA
Tnf	F: GCCTATGTCTCAGCCTCTTCT	*Ogdh*	F: CTCCCAGGGTGTCGTCAATC
	R: CACTTGGTGGTTTGCTACGA		R: TCCAGGGTGAAAAAGCCAGG
Il1b	F: TTCCCCAGGGCATGTTAAGG	*Sdhd*	F: CCAAGCCACCACTCTGGTTC
	R: GTCTTGGCCGAGGACTAAGG		R: GCAGCCAGAGAGTAGTCCAC
Ccl2	F: CTGTAGTTTTTGTCACCAAGCTC	*Uqcrq*	F: GCGCCTTCCCAAGCTATTTC
	R: AGACCTTAGGGCAGATGCAG		R: ACCACTACAAACGGCGGC
Mrc1	F: AATGCTGACCTCCTGAGTGT	*Lcor*	F: GGCTGACCAAGACTCACCTC
	R: CAGTTCAGATACCGGAATGG		R: ACACCGTCTTGTTCACTAGGT
Fizz1	F: CCTGCTGGGATGACTGCTAC	*Ncor2*	F: CATCACTGGAGCAGGCCTTATG
	R: CAGTGGTCCAGTCAACGAGT		R: GGGCTCTTCCCACTGATCATATT
Ym1	F: TCTCAATGTGGATTCAATCATTTCC	*B2m*	F: TCGGTGACCCTGGTCTTTCT
	R: CAGTACTAATTGTAGGGGCACCA		R: TTTGAGGGGTTTTCTGGATAGCA
Sirt1	F: GCGGCTTGAGGGTAATCAAT	*Gapdh*	F: CATGGCCTTCCGTGTTCCTA
	R: ACCTCAGCACCGTGGAATATG		R: CCTGCTTCACCACCTTCTTGAT
Ppargc1b	F: GAAGATCCAAGCTGCCCAC	*Tbp*	F: ACCCTTCACCAATGACTCCTATG
	R: TGCCAAGAGAGTCGCTTTGTG		R: ATGATGACTGCAGCAAATCGC
Acox1	F: CTACGTGCAGCCAGATTGGT	*mt16srRNA*	F: CCGCAAGGGAAAGATGAAAGAC
	R: AAGTTCCACGCCACTTCCTT		R: TCGTTTGGTTTCGGGGTTTC
Acox3	F: CCAAAGCTGATGGTGAGCTCTAT	*hexokinase 2*	F: GCCAGCCTCTCCTGATTTTAGTGT
	R: CTGGGACTTTAGCCTGTCGG		R: GGGAACACAAAAGACCTCTTCTGG
Hadha	F: AAAGGCTTTGAGAAGGCCGA		
	R: TGGAGTCACGCTTTCCACTT		

Supplemental Table 3. Lesion size, leukocyte counts and circulating cholesterol level in *M-Dicer*$^{+/+}$ and *M-Dicer*$^{-/-}$ mice fed the HFD for 12 weeks.

Indices	*M-Dicer*$^{+/+}$ (mean ± SEM)	*M-Dicer*$^{-/-}$ (mean ± SEM)	*P*-value
Lesion size (aorta)	2.11 ± 0.26*	3.26 ± 0.35*	0.01
Lesion size (aortic root)	9.35 ± 0.41†	12.34 ± 1.39†	0.04
Leukocytes	4.29 ± 0.41‡	4.32 ± 0.55‡	0.97
Cholesterol	28.10 ± 1.29§	28.13 ± 1.84§	0.99

*Lesion size in the aorta expressed as percentage of oil-red O positive area in aortic whole area. *n* = 13 or 14 mice per group.
†Lesion size in the aortic root expressed as absolute area (x 10^4 μm^2) per valve. *n* = 8 or 9 mice per group.
‡Peripheral cell counts expressed as cells (x 10^6) per ml of whole blood. *n* = 10 mice per group.
§Circulating cholesterol level expressed as mmol/L. *n* = 8 or 9 mice per group.

Supplemental Table 4. Differentially expressed genes (cutoff: 1.5-fold change, *P* < 0.05, *n* = 3) in *Dicer*$^{-/-}$ BMDMs compared with *Dicer*$^{+/+}$ BMDMs determined by RNA deep sequencing. (See attached supplemental excel file)

Supplemental Table 5. List of the fold change and *P*-value of miRNA expression in *Dicer*$^{-/-}$ BMDMs *versus* *Dicer*$^{+/+}$ BMDMs determined by miRNA qPCR-array. *n* = 3. (See attached supplemental excel file)

Supplemental Table 6. The list of mRNAs that are upregulated (cutoff: 2-fold change) and at least 50% less enriched in AGO2-complexes in *Dicer*$^{-/-}$ BMDMs compared with *Dicer*$^{+/+}$ BMDMs, determined by AGO2-RIP-chip. (See attached supplemental excel file)

Supplemental Table 7. Body weight, leukocyte counts and circulating cholesterol level in *Apoe*$^{-/-}$ mice treated with control (ctrl) or miR10a/*Lcor* TSBs during 12-week HFD feeding program.

Indices	ctrl TSB (mean ± SEM) *n* = 6	miR10a/*Lcor* TSB (mean ± SEM) *n* = 7	*P*-value
Weight (g)	34.00 ± 0.86	32.86 ± 0.59	0.29
Leukocytes	5.85 ± 0.66*	5.98 ± 0.96*	0.36
Cholesterol	31.87 ± 1.76†	30.41 ± 1.40†	0.52

*Peripheral cell counts expressed as cells (x 10^6) per ml of whole blood.
†Circulating cholesterol level expressed as mmol/L.

Supplemental Figures

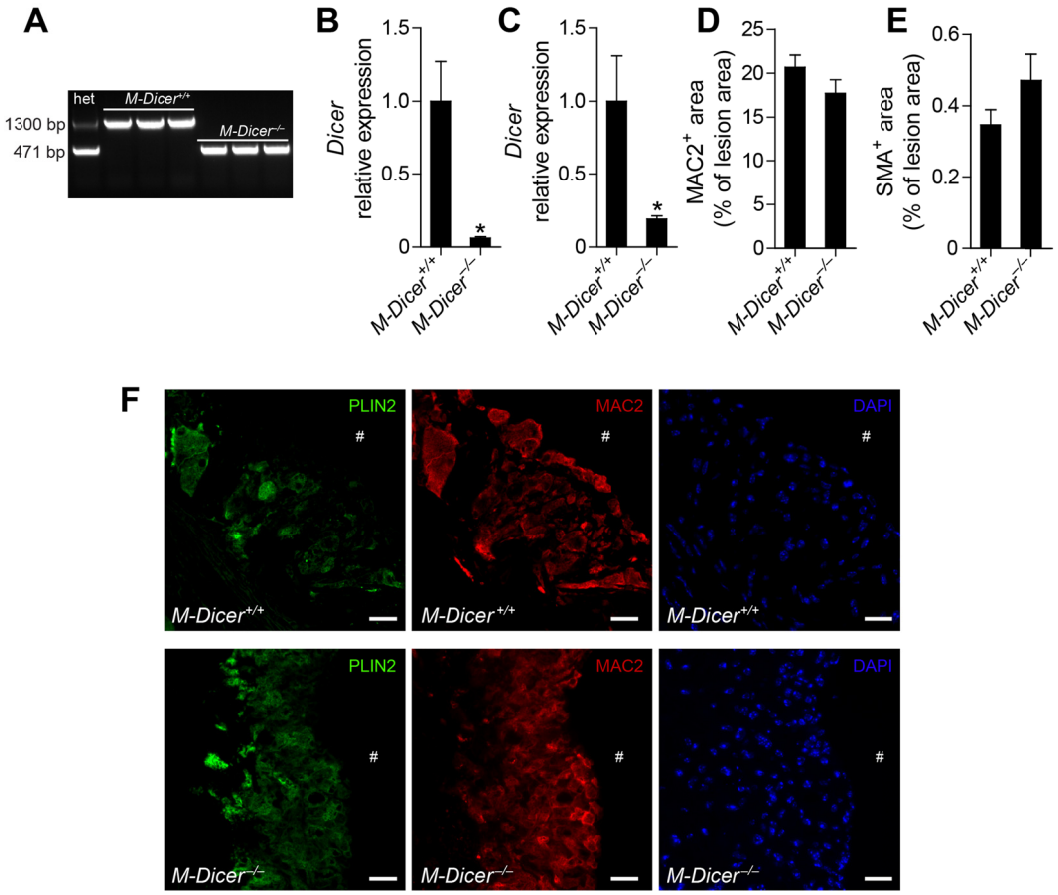

Supplemental Figure 1. Deletion of *Dicer* in macrophages has no effect on lesional macrophage and smooth muscle cell contents. (A) The *Dicer* allele was genotyped in bone marrow-derived macrophages (BMDMs) from *M-Dicer*$^{+/-}$ (het), *M-Dicer*$^{+/+}$ and M-*Dicer*$^{-/-}$ mice. The deletion allele produced a 471-bp PCR product whereas a wild-type allele resulted in a 1,300-bp product. (B) The mRNA level of *Dicer* in BMDMs from *M-Dicer*$^{+/+}$ and M-*Dicer*$^{-/-}$ mice. *n* = 3. (C) The mRNA level of *Dicer* in atherosclerotic lesions collected via laser capture microdissection from aortic arch of *M-Dicer*$^{+/+}$ and M-*Dicer*$^{-/-}$ mice fed the high-fat diet (HFD) for 12 weeks. *n* = 5 or 6 mice per group. (D,E) Quantification of lesional macrophages (D) and smooth muscle cells (E) in aortic roots from *M-Dicer*$^{+/+}$ and M-*Dicer*$^{-/-}$ mice fed the HFD for 12 weeks determined by MAC2 and α-smooth muscle actin (SMA) immunostaining, respectively. *n* = 8–10 mice per group. (F) Representative images of PLIN2 and MAC2 immunostainings in aortic roots from *M-Dicer*$^{+/+}$ and M-*Dicer*$^{-/-}$ mice fed the HFD for 12 week.

Scale bars, 20 μm. *n* = 8 mice per group. # indicates the lumen. The data in B–E are represented as mean ± SEM (*$P < 0.05$ by Student's t test).

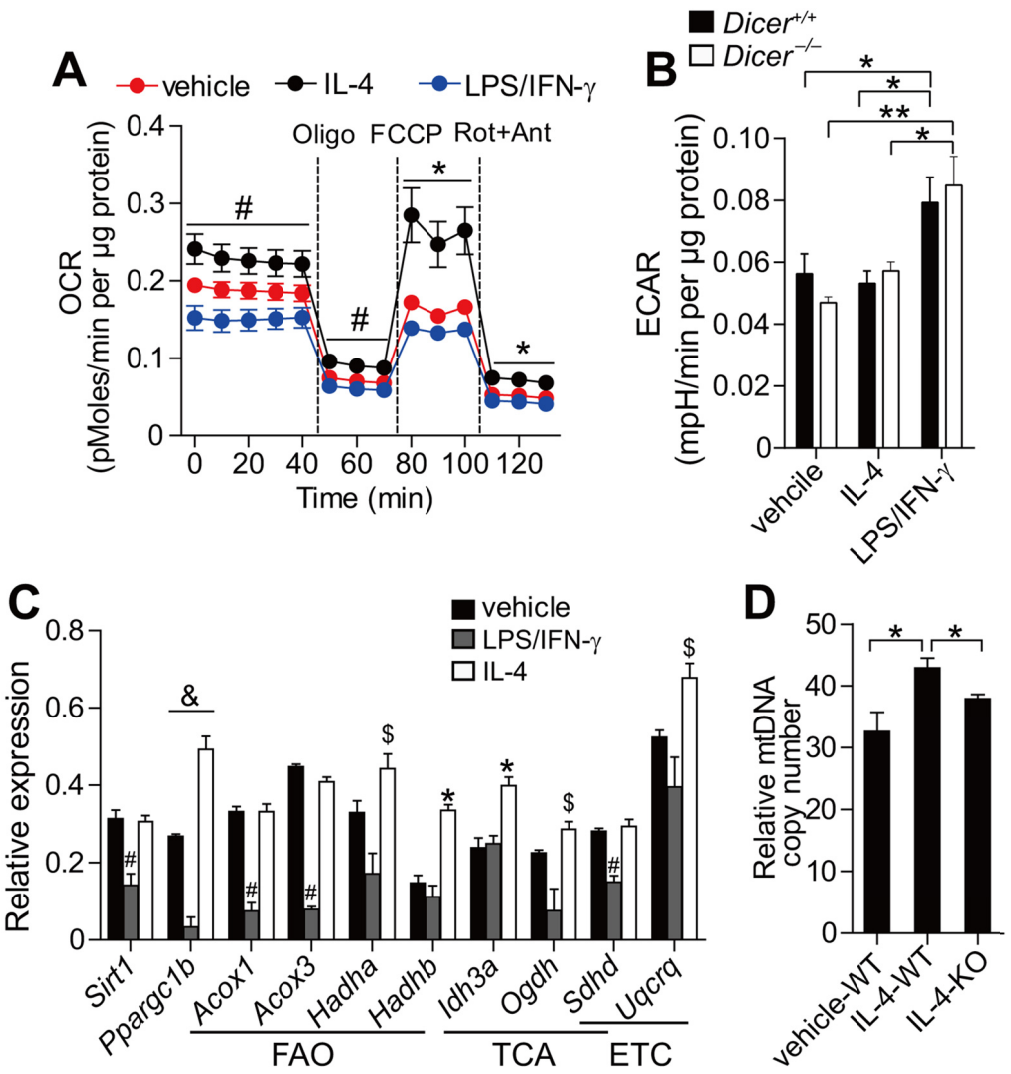

Supplemental Figure 2. Dicer promotes mitochondrial oxidative metabolism during IL-4-stimulated alternative macrophage activation. (A) Oxygen consumption rate (OCR) at basal condition and after the sequential treatment with oligomycin (Oligo), FCCP and rotenone plus antimycin (Rot+Ant) in *Dicer*$^{+/+}$ BMDMs treated with vehicle, IL-4 or LPS/IFN-γ. *n* = 3 or 4; **P* < 0.05 IL-4 *versus* vehicle and LPS/IFN-γ and $^{\#}$*P* < 0.05 IL-4 *versus* LPS/IFN-γ by one-way ANOVA followed by Tukey-Kramer test. (B) The extracellular acidification rate (ECAR) of *Dicer*$^{+/+}$ or *Dicer*$^{-/-}$ BMDMs treated with vehicle, IL-4 or LPS/IFN-γ. *n* = 6; **P* < 0.05 by two-way ANOVA followed by Tukey-Kramer test. (C) Relative mRNA levels of genes related to mitochondrial oxidative metabolism in *Dicer*$^{+/+}$ BMDMs treated with vehicle, IL-4 or LPS/IFN-γ. *n* = 3 or 4; $^{\#}$*P* < 0.05 *versus* vehicle and IL-4, $^{\$}$*P* < 0.05 *versus* LPS/IFN-γ, **P* < 0.05 *versus* vehicle and LPS/IFN-γ, $^{\&}$*P* < 0.05 in all three groups by one-way ANOVA

followed by Tukey-Kramer test. FAO, fatty acid oxidation; TCA, tricarboxylic acid cycle; ETC, electron transport chain. (D) Mitochondrial DNA (mtDNA) copy number was measured in vehicle- or IL-4-treated *Dicer*$^{+/+}$ (WT) or *Dicer*$^{-/-}$ (KO) BMDMs by quantitative PCR and normalized to nuclear DNA levels in a ration of mtDNA 16srRNA over nuclear hexokinase 2. n = 3 or 4; *P < 0.05 by one-way ANOVA followed by Fisher's LSD test. All data are represented as mean ± SEM.

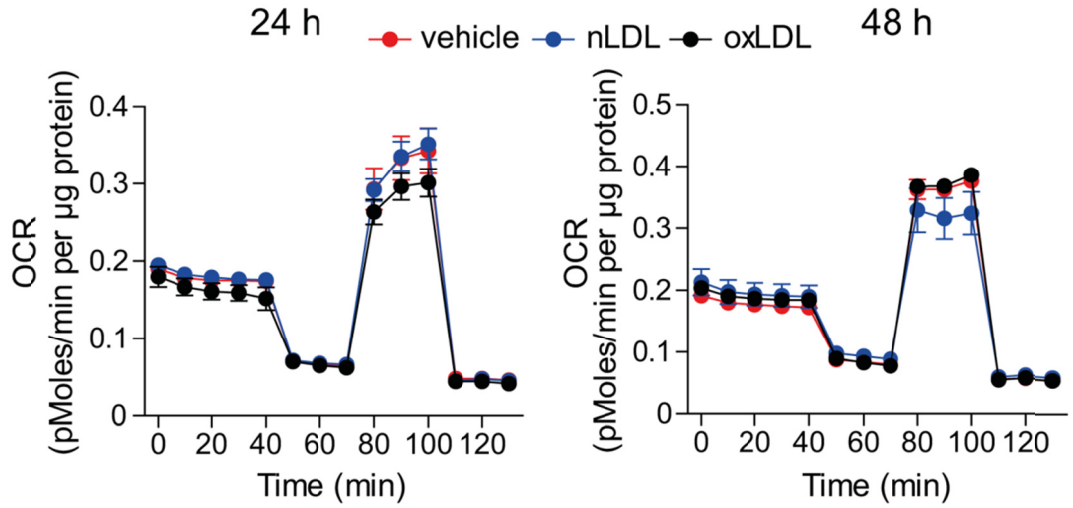

Supplemental Figure 3. Short time treatment with oxidized low-density lipoprotein (oxLDL) has no effect on oxygen consumption in macrophages. *Dicer*$^{+/+}$ BMDMs were treated with vehicle, native LDL (nLDL) or oxLDL for 24 or 48 hours and the OCR was measured at basal condition and after the sequential treatment with oligomycin (Oligo), FCCP and rotenone plus antimycin (Rot+Ant). *n* = 4 or 5.

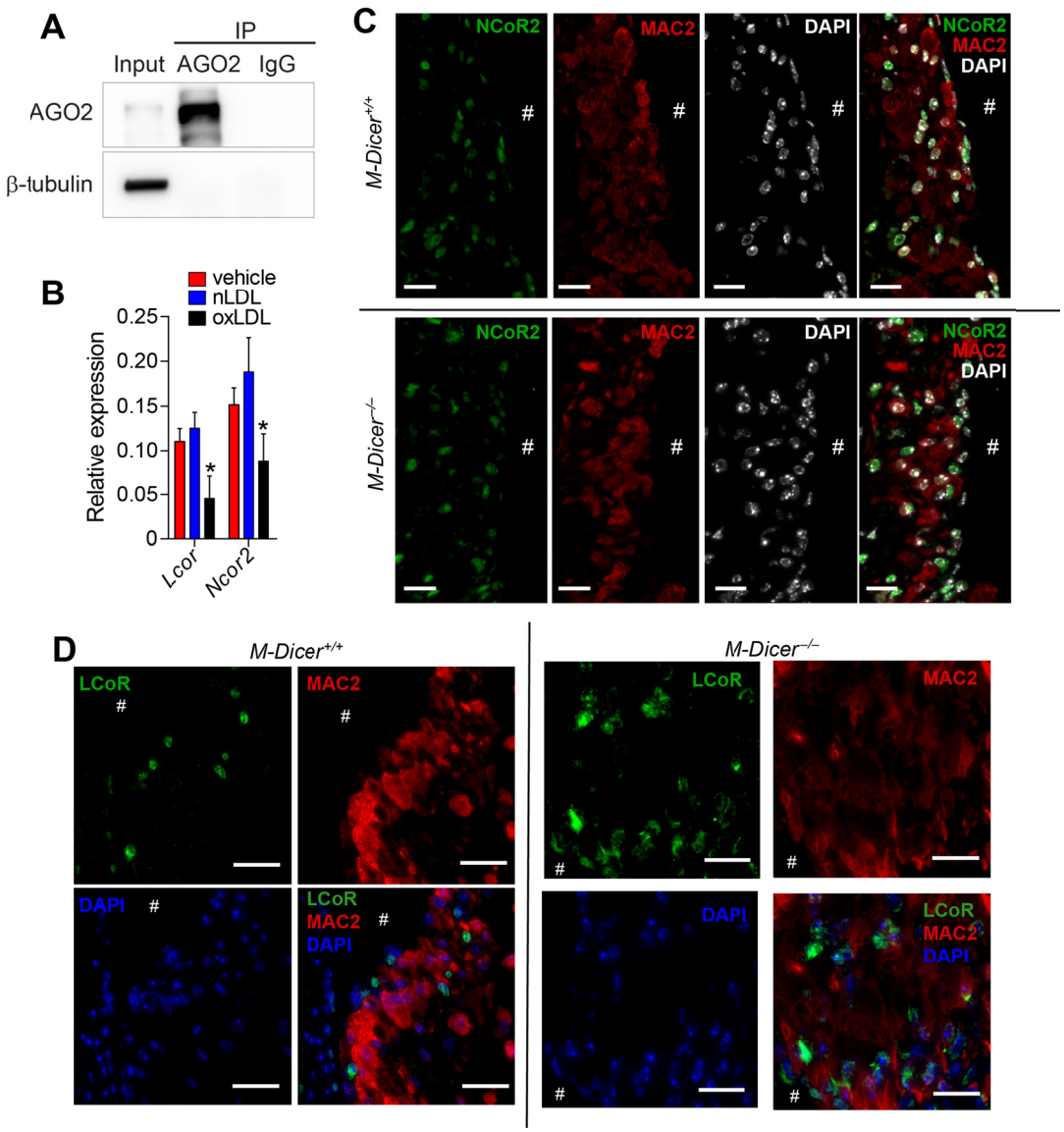

Supplemental Figure 4. Expression patterns of Lcor and Ncor2. (A) Enrichment of AGO2 protein in the AGO2-IP samples, but not in the IgG-IP samples, demonstrated by Western blot. (B) Relative mRNA levels of *Lcor* and *Ncor2* in *Dicer*$^{+/+}$ BMDMs treated with vehicle, nLDL or oxLDL for 72 h. *n* = 3 or 4. Data are represented as mean ± SEM. **P* < 0.05 *versus* nLDL by one-way ANOVA followed by Fisher's LSD test. (C) Double immunostaining for NCoR2 (green) and MAC2 (red) in aortic roots from *M-Dicer*$^{+/+}$ and *M-Dicer*$^{–/–}$ mice fed the HFD for 12 weeks. Nuclei were stained with DAPI. Scale bars: 20 μm. # indicates the lumen. (D) Double immunostaining for LCoR (green) and MAC2 (red) in aortic roots from *M-Dicer*$^{+/+}$ and *M-Dicer*$^{–/–}$ mice fed the HFD for 12 weeks. Nuclei were stained with DAPI. Scale bars: 20 μm. # indicates the lumen.

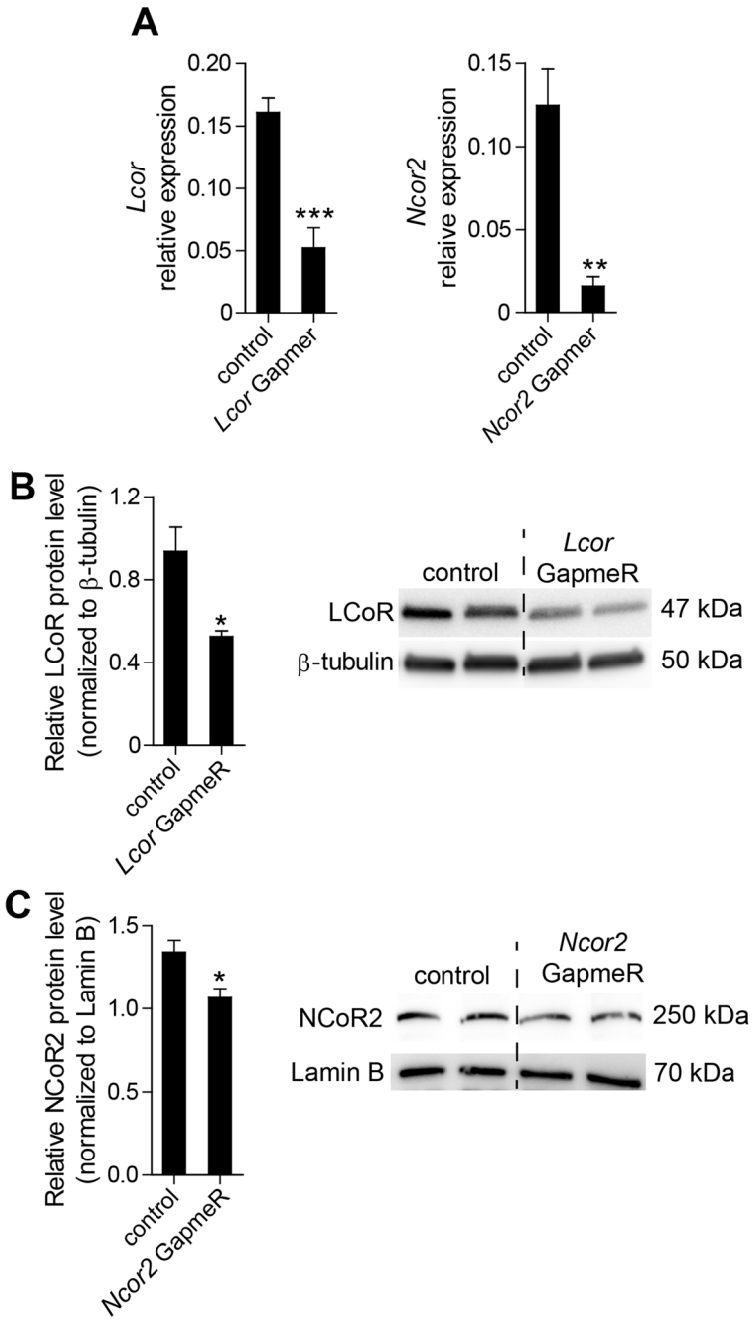

Supplemental Figure 5. Silencing of Lcor and Ncor2 using GapmeRs. *Lcor* and *Ncor2* GapmeRs reduced the Lcor and Ncor2 expression, respectively, at the mRNA (A, $n = 5$) and at the protein level (B and C, $n = 4$) in IL-4-stimulated *Dicer*$^{-/-}$ BMDMs compared with control GapmeR treatment. All data are represented as mean ± SEM (*$P < 0.05$, **$P < 0.005$ and ***$P < 0.001$ by Student's t-test).

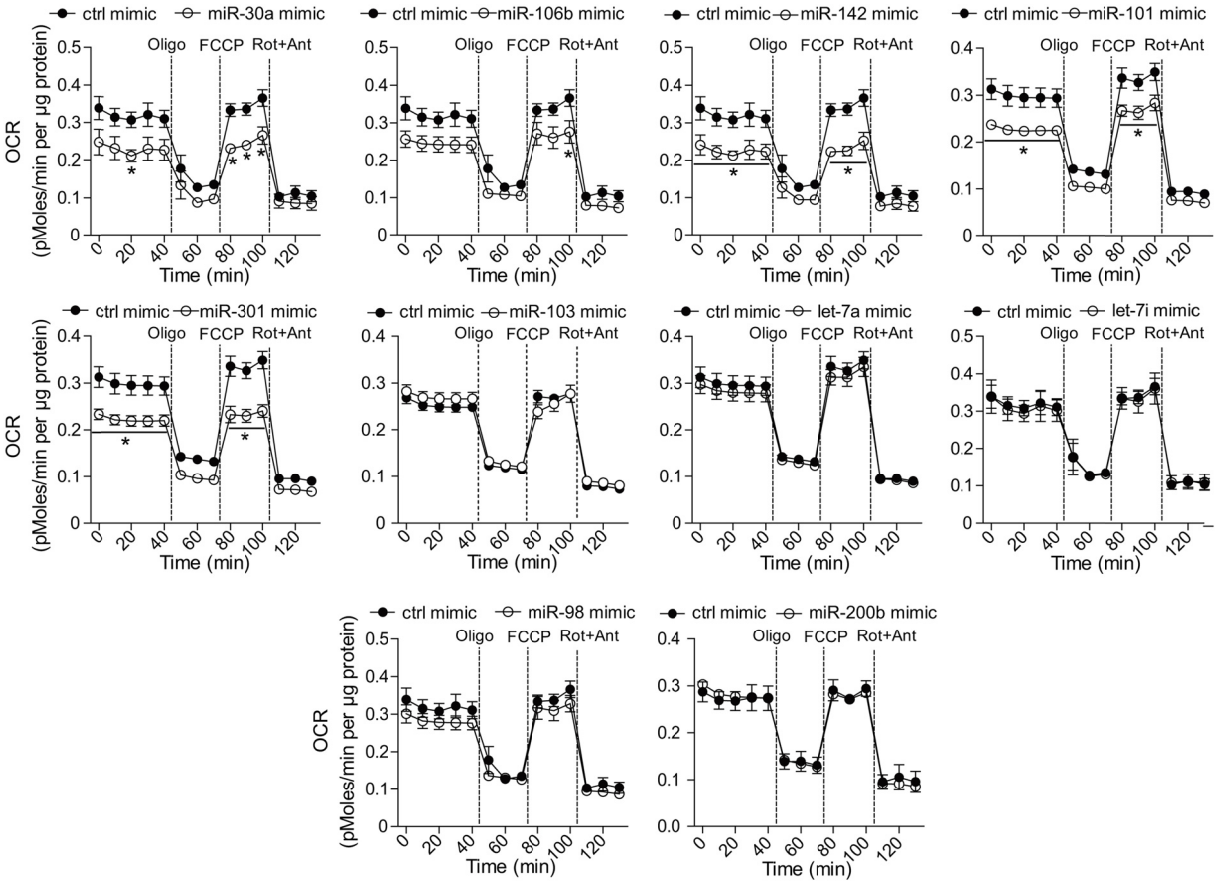

Supplemental Figure 6. The role of miRNAs that are predicted to target Lcor or Ncor2 in Dicer-promoted mitochondrial oxidative metabolism. OCR of *Dicer*$^{-/-}$ BMDMs transfected with the mimics of *Lcor*- or *Ncor2*-targeting miRNAs or scrambled control in the presence of IL-4. *n* = 4 or 5. All data are represented as mean ± SEM (**P* < 0.05 by Student's t-test).

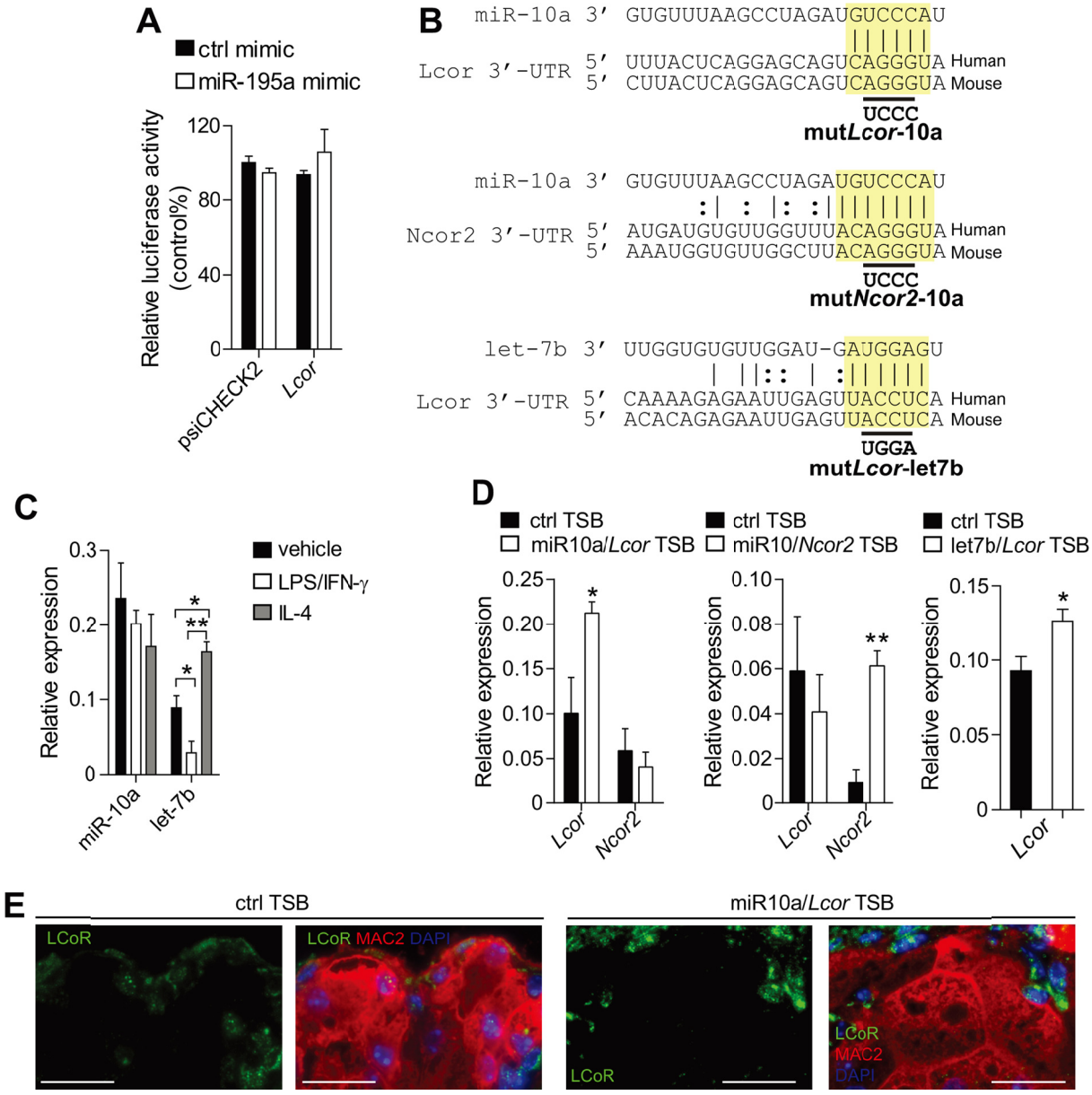

Supplemental Figure 7. Targeting of Lcor and Ncor2 by miRNAs. (A) Relative luciferase activity in HEK293 cells co-transfected with the psiCHECK2 vector or the psiCHECK2 vector containing wild-type *Lcor* 3′-untranslated region (UTR) and miR-195 or control (ctrl) mimics. *n* = 5 or 6. (B) Sequence alignment of miR-10a and its predicted binding site in the 3′-UTR of human and mouse *Lcor* and *Ncor2*, and of let-7b and its predicted binding site in the 3′-UTR of human and mouse *Lcor*. Mutations in the mouse 3′-UTRs (bold) were introduced into the region complementary to the seed regions of miR-10a or let-7b (yellow). (C) The miR-10a and let-7b expression levels in *Dicer*$^{+/+}$ BMDMs treated with vehicle, LPS/IFN-γ or IL-4. *n* = 3.

(D) The mRNA levels of *Lcor* in *Dicer*$^{+/+}$ BMDMs transfected with miR10a/*Lcor*, miR10a/*Ncor2,* let7b/*Lcor* or control (ctrl) TSBs, and of *Ncor2* in *Dicer*$^{+/+}$ BMDMs transfected with miR10a/*Lcor*, miR10a/*Ncor2* or ctrl TSBs. *n* = 4 or 5. (E) Representative images of combined LCoR (green) and MAC2 (red) immunostaining in aortic roots from *Apoe*$^{-/-}$ mice injected with control (ctrl) or miR10a/Lcor TSBs after a 12-week HFD programme. Nuclei were stained with DAPI. Scale bars: 20 μm. The data in A, C and D are represented as mean ± SEM. **P* < 0.05 and ***P* < 0.005.

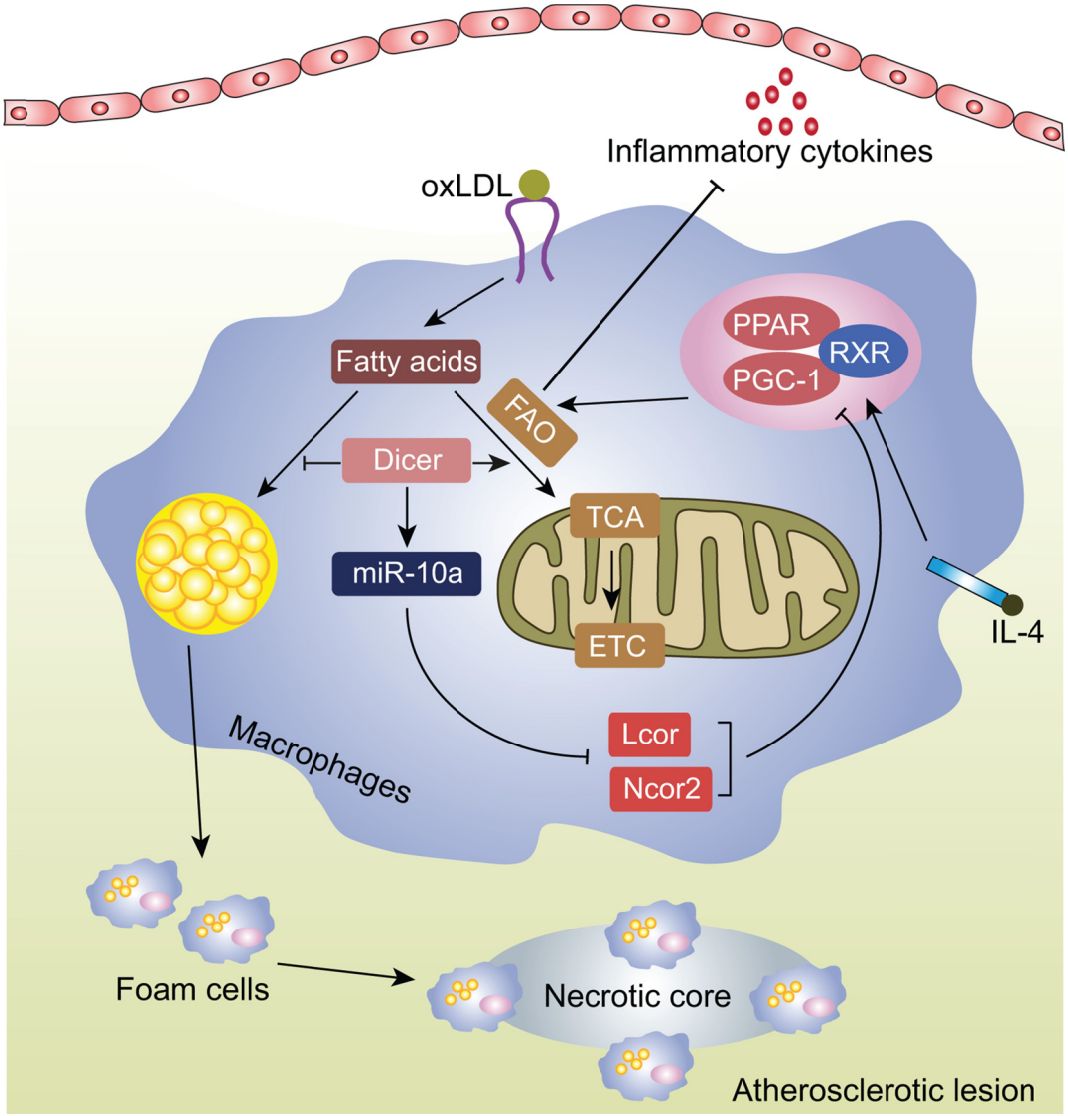

Supplemental Figure 8. Schematic showing the proposed model of miRNA-regulated metabolic reprogramming essential for alternative macrophage activation and lipid metabolism in macrophages, which plays an atheroprotective role. Dicer promotes mitochondrial fatty acid oxidation (FAO) and oxidative phosphorylation by generating miR-10a. miR-10a targets nuclear receptor co-repressors, Lcor or Ncor2, thus activating PPAR/RXR/PGC1 signaling which mediates Dicer-dependent mitochondrial oxidative metabolism. Dicer-promoted metabolic reprograming results in alternative activation, and inhibits cell death and lipid accumulation in macrophages, therefore limiting atherosclerosis by inhibiting inflammatory response, reducing foam cell accumulation and decreasing necrotic core formation. IL-4, interleukin 4; oxLDL, oxidized low-density lipoprotein; TCA, tricarboxylic acid cycle; ETC, electron transport chain.

Supplemental References

1. Harfe BD, McManus MT, Mansfield JH, Hornstein E, Tabin CJ. The rnaseiii enzyme dicer is required for morphogenesis but not patterning of the vertebrate limb. *Proc. Natl. Acad. Sci. U. S. A*. 2005;102:10898-10903. doi: 10.1073/pnas.0504834102.
2. Akhtar S, Gremse F, Kiessling F, Weber C, Schober A. Cxcl12 promotes the stabilization of atherosclerotic lesions mediated by smooth muscle progenitor cells in apoe-deficient mice. *Arterioscler. Thromb. Vasc. Biol*. 2013;33:679-686. doi: 10.1161/ATVBAHA.112.301162.
3. Wei Y, Nazari-Jahantigh M, Chan L, Zhu M, Heyll K, Corbalan-Campos J, Hartmann P, Thiemann A, Weber C, Schober A. The microrna-342-5p fosters inflammatory macrophage activation through an akt1- and microrna-155-dependent pathway during atherosclerosis. *Circulation*. 2013;127:1609-1619. doi: 10.1161/CIRCULATIONAHA.112.000736.
4. Nuovo G, Lee EJ, Lawler S, Godlewski J, Schmittgen T. In situ detection of mature micrornas by labeled extension on ultramer templates. *BioTechniques*. 2009;46:115-126. doi: 10.2144/000113068.
5. Schober A, Nazari-Jahantigh M, Wei Y, Bidzhekov K, Gremse F, Grommes J, Megens RT, Heyll K, Noels H, Hristov M, Wang S, Kiessling F, Olson EN, Weber C. Microrna-126-5p promotes endothelial proliferation and limits atherosclerosis by suppressing dlk1. *Nat. Med.* 2014;20:368-376. doi: 10.1038/nm.3487.
6. Wei Y, Zhu M, Corbalan-Campos J, Heyll K, Weber C, Schober A. Regulation of csf1r and bcl6 in macrophages mediates the stage-specific effects of microrna-155 on atherosclerosis. *Arterioscler. Thromb. Vasc. Biol*. 2015;35:796-803. doi: 10.1161/ATVBAHA.114.304723.